The Pierre Auger Observatory and its Upgrade

The Pierre Auger Collaboration*:

A. Aab[76], P. Abreu[68], M. Aglietta[51,50], J.M. Albury[12], I. Allekotte[1], A. Almela[8,11], J. Alvarez-Muñiz[75], R. Alves Batista[76], G.A. Anastasi[59,50], L. Anchordoqui[83], B. Andrada[8], S. Andringa[68], C. Aramo[48], P.R. Araújo Ferreira[40], H. Asorey[8], P. Assis[68], G. Avila[10], A.M. Badescu[71], A. Bakalova[30], A. Balaceanu[69], F. Barbato[57,48], R.J. Barreira Luz[68], K.H. Becker[36], J.A. Bellido[12], C. Berat[34], M.E. Bertaina[59,50], X. Bertou[1], P.L. Biermann[c], T. Bister[40], J. Biteau[35], J. Blazek[30], C. Bleve[34], M. Boháčová[30], D. Boncioli[54,44], C. Bonifazi[24], L. Bonneau Arbeletche[19], N. Borodai[65], A.M. Botti[8], J. Brack[h], T. Bretz[40], F.L. Briechle[40], P. Buchholz[42], A. Bueno[74], S. Buitink[14], M. Buscemi[55,45], K.S. Caballero-Mora[63], L. Caccianiga[56,47], A. Cancio[11,8], F. Canfora[76,78], I. Caracas[36], J.M. Carceller[74], R. Caruso[55,45], A. Castellina[51,50], F. Catalani[17], G. Cataldi[46], L. Cazon[68], M. Cerda[9], J.A. Chinellato[20], K. Choi[13], J. Chudoba[30], L. Chytka[31], R.W. Clay[12], A.C. Cobos Cerutti[7], R. Colalillo[57,48], A. Coleman[89], M.R. Coluccia[53,46], R. Conceição[68], A. Condorelli[43,44], G. Consolati[47,52], F. Contreras[10], F. Convenga[53,46], C.E. Covault[81,e], S. Dasso[5,3], K. Daumiller[38], B.R. Dawson[12], J.A. Day[12], R.M. de Almeida[26], J. de Jesús[8,38], S.J. de Jong[76,78], G. De Mauro[76,78], J.R.T. de Mello Neto[24,25], I. De Mitri[43,44], J. de Oliveira[26], D. de Oliveira Franco[20], V. de Souza[18], E. De Vito[53,46], J. Debatin[37], M. del Río[10], O. Deligny[32], N. Dhital[65], A. Di Matteo[50], C. Dobrigkeit[20], J.C. D'Olivo[64], R.C. dos Anjos[23], M.T. Dova[4], J. Ebr[30], R. Engel[37,38], I. Epicoco[53,46], M. Erdmann[40], C.O. Escobar[a], A. Etchegoyen[8,11], H. Falcke[76,79,78], J. Farmer[88], G. Farrar[86], A.C. Fauth[20], N. Fazzini[f], F. Feldbusch[39], F. Fenu[59,50], B. Fick[85], J.M. Figueira[8], A. Filipčič[73,72], T. Fodran[76], M.M. Freire[6], T. Fujii[88,i], A. Fuster[8,11], C. Galea[76], C. Galelli[56,47], B. García[7], A.L. Garcia Vegas[40], H. Gemmeke[39], F. Gesualdi[8,38], A. Gherghel-Lascu[69], P.L. Ghia[32], U. Giaccari[76], M. Giammarchi[47], M. Giller[66], J. Glombitza[40], F. Gobbi[9], F. Gollan[8], G. Golup[1], M. Gómez Berisso[1], P.F. Gómez Vitale[10], J.P. Gongora[10], N. González[8], I. Goos[1,38], D. Góra[65], A. Gorgi[51,50], M. Gottowik[36], T.D. Grubb[12], F. Guarino[57,48], G.P. Guedes[21], E. Guido[50,59], S. Hahn[38,8], R. Halliday[81], M.R. Hampel[8], P. Hansen[4], D. Harari[1], V.M. Harvey[12], A. Haungs[38], T. Hebbeker[40], D. Heck[38], G.C. Hill[12], C. Hojvat[f], J.R. Hörandel[76,78], P. Horvath[31], M. Hrabovský[31], T. Huege[38,14], J. Hulsman[8,38], A. Insolia[55,45], P.G. Isar[70], J.A. Johnsen[82], J. Jurysek[30], A. Kääpä[36], K.H. Kampert[36], B. Keilhauer[38], J. Kemp[40], H.O. Klages[38], M. Kleifges[39], J. Kleinfeller[9], M. Köpke[37], G. Kukec Mezek[72], B.L. Lago[16], D. LaHurd[81], R.G. Lang[18], N. Langner[40], M.A. Leigui de Oliveira[22], V. Lenok[38], A. Letessier-Selvon[33], I. Lhenry-Yvon[32], D. Lo Presti[55,45], L. Lopes[68], R. López[60], R. Lorek[81], Q. Luce[37], A. Lucero[8], J.P. Lundquist[72], A. Machado Payeras[20], G. Mancarella[53,46], D. Mandat[30], B.C. Manning[12], J. Manshanden[41], P. Mantsch[f], S. Marafico[32], A.G. Mariazzi[4], I.C. Mariş[13], G. Marsella[53,46], D. Martello[53,46], H. Martinez[18], O. Martínez Bravo[60], M. Mastrodicasa[54,44], H.J. Mathes[38], J.Matthews[84], G. Matthiae[58,49], E. Mayotte[36], P.O. Mazur[f], G. Medina-Tanco[64], D. Melo[8], A. Menshikov[39], K.-D. Merenda[82], S. Michal[31], M.I. Micheletti[6], L. Miramonti[56,47], S. Mollerach[1], F. Montanet[34], C. Morello[51,50], M. Mostafá[87], A.L. Müller[8,38], M.A. Muller[20,b,24], K. Mulrey[14], R. Mussa[50], M. Muzio[86], W.M. Namasaka[36], L. Nellen[64], M. Niculescu-Oglinzanu[69], M. Niechciol[42], D. Nitz[85,g], D. Nosek[29], V. Novotny[29], L. Nožka[31], A Nucita[53,46], L.A. Núñez[28], M. Palatka[30], J. Pallotta[2], P. Papenbreer[36], G. Parente[75], A. Parra[60], M. Pech[30], F. Pedreira[75], J. Pękala[65], R. Pelayo[62], J. Peña-Rodriguez[28], J. Perez Armand[19], M. Perlin[8,38], L. Perrone[53,46], S. Petrera[43,44], T. Pierog[38], M. Pimenta[68], V. Pirronello[55,45], M. Platino[8], B. Pont[76], M. Pothast[78,76], P. Privitera[88], M. Prouza[30], A. Puyleart[85], S. Querchfeld[36], J. Rautenberg[36], D. Ravignani[8], M. Reininghaus[38,8], J. Ridky[30], F. Riehn[68], M. Risse[42], P. Ristori[2], V. Rizi[54,44], W. Rodrigues de Carvalho[19], J. Rodriguez Rojo[10], M.J. Roncoroni[8], M. Roth[38], E. Roulet[1], A.C. Rovero[5], P. Ruehl[42], S.J. Saffi[12], A. Saftoiu[69], F. Salamida[54,44], H. Salazar[60], G. Salina[49], J.D. Sanabria Gomez[28], F. Sánchez[8], E.M. Santos[19], E. Santos[30], F. Sarazin[82], R. Sarmento[68], C. Sarmiento-Cano[8], R. Sato[10], P. Savina[53,46,32], C.M. Schäfer[38], V. Scherini[46], H. Schieler[38], M. Schimassek[37,8], M. Schimp[36], F. Schlüter[38,8], D. Schmidt[37], O. Scholten[77,14], P. Schovánek[30], F.G. Schröder[89,38], S. Schröder[36], J. Schulte[40], S.J. Sciutto[4], M. Scornavacche[8,38], R.C. Shellard[15], G. Sigl[41], G. Silli[8,38], O. Sima[69,j], R.Šmída[88], P. Sommers[87], J.F. Soriano[83], J. Souchard[34], R. Squartini[9], M. Stadelmaier[38,8], D. Stanca[69], S. Stanič[72], J. Stasielak[65], P. Stassi[34],

A. Streich[37,8], M. Suárez-Durán[28], T. Sudholz[12], T. Suomijärvi[35], A.D. Supanitsky[8], J.Šupík[31], Z. Szadkowski[67], A. Taboada[37], A. Tapia[27], C. Timmermans[78,76], O. Tkachenko[38], P. Tobiska[30], C.J. Todero Peixoto[17], B. Tomé[68], A. Travaini[9], P. Travnicek[30], C. Trimarelli[54,44], M. Trini[72], M. Tueros[4], R. Ulrich[38], M. Unger[38], L. Vaclavek[31], M. Vacula[31], J.F. Valdés Galicia[64], L. Valore[57,48], E. Varela[60], V. Varma K.C.[8,38], A. Vásquez-Ramírez[28], D. Veberič[38], C. Ventura[25], I.D. Vergara Quispe[4], V. Verzi[49], J. Vicha[30], J. Vink[80], S. Vorobiov[72], H. Wahlberg[4], A.A. Watson[d], M. Weber[39], A. Weindl[38], L. Wiencke[82], H. Wilczyński[65], T. Winchen[14], M. Wirtz[40], D. Wittkowski[36], B. Wundheiler[8], A. Yushkov[30], O. Zapparrata[13], E. Zas[75], D. Zavrtanik[72,73], M. Zavrtanik[73,72], L. Zehrer[72], A. Zepeda[61]

[1] *Centro Atómico Bariloche and Instituto Balseiro (CNEA-UNCuyo-CONICET), San Carlos de Bariloche, Argentina*
[2] *Centro de Investigaciones en Láseres y Aplicaciones, CITEDEF and CONICET, Villa Martelli, Argentina*
[3] *Departamento de Física and Departamento de Ciencias de la Atmósfera y los Océanos, FCEyN, Universidad de Buenos Aires and CONICET, Buenos Aires, Argentina*
[4] *IFLP, Universidad Nacional de La Plata and CONICET, La Plata, Argentina*
[5] *Instituto de Astronomía y Física del Espacio (IAFE, CONICET-UBA), Buenos Aires, Argentina*
[6] *Instituto de Física de Rosario (IFIR) – CONICET/U.N.R. and Facultad de Ciencias Bioquímicas y Farmacéuticas U.N.R., Rosario, Argentina*
[7] *Instituto de Tecnologías en Detección y Astropartículas (CNEA, CONICET, UNSAM), and Universidad Tecnológica Nacional – Facultad Regional Mendoza (CONICET/CNEA), Mendoza, Argentina*
[8] *Instituto de Tecnologías en Detección y Astropartículas (CNEA, CONICET, UNSAM), Buenos Aires, Argentina*
[9] *Observatorio Pierre Auger, Malargüe, Argentina*
[10] *Observatorio Pierre Auger and Comisión Nacional de Energía Atómica, Malargüe, Argentina*
[11] *Universidad Tecnológica Nacional – Facultad Regional Buenos Aires, Buenos Aires, Argentina*
[12] *University of Adelaide, Adelaide, S.A., Australia*
[13] *Université Libre de Bruxelles (ULB), Brussels, Belgium*
[14] *Vrije Universiteit Brussels, Brussels, Belgium*
[15] *Centro Brasileiro de Pesquisas Fisicas, Rio de Janeiro, RJ, Brazil*
[16] *Centro Federal de Educação Tecnológica Celso Suckow da Fonseca, Nova Friburgo, Brazil*
[17] *Universidade de São Paulo, Escola de Engenharia de Lorena, Lorena, SP, Brazil*
[18] *Universidade de São Paulo, Instituto de Física de São Carlos, São Carlos, SP, Brazil*
[19] *Universidade de São Paulo, Instituto de Física, São Paulo, SP, Brazil*
[20] *Universidade Estadual de Campinas, IFGW, Campinas, SP, Brazil*
[21] *Universidade Estadual de Feira de Santana, Feira de Santana, Brazil*
[22] *Universidade Federal do ABC, Santo André, SP, Brazil*
[23] *Universidade Federal do Paraná, Setor Palotina, Palotina, Brazil*
[24] *Universidade Federal do Rio de Janeiro, Instituto de Física, Rio de Janeiro, RJ, Brazil*
[25] *Universidade Federal do Rio de Janeiro (UFRJ), Observatório do Valongo, Rio de Janeiro, RJ, Brazil*
[26] *Universidade Federal Fluminense, EEIMVR, Volta Redonda, RJ, Brazil*
[27] *Universidad de Medellín, Medellín, Colombia*
[28] *Universidad Industrial de Santander, Bucaramanga, Colombia*
[29] *Charles University, Faculty of Mathematics and Physics, Institute of Particle and Nuclear Physics, Prague, Czech Republic*
[30] *Institute of Physics of the Czech Academy of Sciences, Prague, Czech Republic*
[31] *Palacky University, RCPTM, Olomouc, Czech Republic*
[32] *CNRS/IN2P3, IJCLab, Université Paris-Saclay, Orsay, France*
[33] *Laboratoire de Physique Nucléaire et de Hautes Energies (LPNHE), Sorbonne Université, Université de Paris, CNRS-IN2P3, Paris, France*
[34] *Univ. Grenoble Alpes, CNRS, Grenoble Institute of Engineering Univ. Grenoble Alpes, LPSC-IN2P3, 38000 Grenoble, France, France*
[35] *Université Paris-Saclay, CNRS/IN2P3, IJCLab, Orsay, France, France*
[36] *Bergische Universität Wuppertal, Department of Physics, Wuppertal, Germany*
[37] *Karlsruhe Institute of Technology, Institute for Experimental Particle Physics (ETP), Karlsruhe, Germany*
[38] *Karlsruhe Institute of Technology, Institut für Kernphysik, Karlsruhe, Germany*
[39] *Karlsruhe Institute of Technology, Institut für Prozessdatenverarbeitung und Elektronik, Karlsruhe, Germany*
[40] *RWTH Aachen University, III. Physikalisches Institut A, Aachen, Germany*
[41] *Universität Hamburg, II. Institut für Theoretische Physik, Hamburg, Germany*
[42] *Universität Siegen, Fachbereich 7 Physik – Experimentelle Teilchenphysik, Siegen, Germany*
[43] *Gran Sasso Science Institute, L'Aquila, Italy*
[44] *INFN Laboratori Nazionali del Gran Sasso, Assergi (L'Aquila), Italy*
[45] *INFN, Sezione di Catania, Catania, Italy*
[46] *INFN, Sezione di Lecce, Lecce, Italy*
[47] *INFN, Sezione di Milano, Milano, Italy*
[48] *INFN, Sezione di Napoli, Napoli, Italy*
[49] *INFN, Sezione di Roma "Tor Vergata", Roma, Italy*
[50] *INFN, Sezione di Torino, Torino, Italy*
[51] *Osservatorio Astrofisico di Torino (INAF), Torino, Italy*

[52] *Politecnico di Milano, Dipartimento di Scienze e Tecnologie Aerospaziali , Milano, Italy*
[53] *Università del Salento, Dipartimento di Matematica e Fisica "E. De Giorgi", Lecce, Italy*
[54] *Università dell'Aquila, Dipartimento di Scienze Fisiche e Chimiche, L'Aquila, Italy*
[55] *Università di Catania, Dipartimento di Fisica e Astronomia, Catania, Italy*
[56] *Università di Milano, Dipartimento di Fisica, Milano, Italy*
[57] *Università di Napoli "Federico II", Dipartimento di Fisica "Ettore Pancini", Napoli, Italy*
[58] *Università di Roma "Tor Vergata", Dipartimento di Fisica, Roma, Italy*
[59] *Università Torino, Dipartimento di Fisica, Torino, Italy*
[60] *Benemérita Universidad Autónoma de Puebla, Puebla, México*
[61] *Centro de Investigación y de Estudios Avanzados del IPN (CINVESTAV), México, D.F., México*
[62] *Unidad Profesional Interdisciplinaria en Ingeniería y Tecnologías Avanzadas del Instituto Politécnico Nacional (UPIITA-IPN), México, D.F., México*
[63] *Universidad Autónoma de Chiapas, Tuxtla Gutiérrez, Chiapas, México*
[64] *Universidad Nacional Autónoma de México, México, D.F., México*
[65] *Institute of Nuclear Physics PAN, Krakow, Poland*
[66] *University of Łódź, Faculty of Astrophysics, Łódź, Poland*
[67] *University of Łódź, Faculty of High-Energy Astrophysics,Łódź, Poland*
[68] *Laboratório de Instrumentação e Física Experimental de Partículas – LIP and Instituto Superior Técnico – IST, Universidade de Lisboa – UL, Lisboa, Portugal*
[69] *"Horia Hulubei" National Institute for Physics and Nuclear Engineering, Bucharest-Magurele, Romania*
[70] *Institute of Space Science, Bucharest-Magurele, Romania*
[71] *University Politehnica of Bucharest, Bucharest, Romania*
[72] *Center for Astrophysics and Cosmology (CAC), University of Nova Gorica, Nova Gorica, Slovenia*
[73] *Experimental Particle Physics Department, J. Stefan Institute, Ljubljana, Slovenia*
[74] *Universidad de Granada and C.A.F.P.E., Granada, Spain*
[75] *Instituto Galego de Física de Altas Enerxías (IGFAE), Universidade de Santiago de Compostela, Santiago de Compostela, Spain*
[76] *IMAPP, Radboud University Nijmegen, Nijmegen, The Netherlands*
[77] *KVI – Center for Advanced Radiation Technology, University of Groningen, Groningen, The Netherlands*
[78] *Nationaal Instituut voor Kernfysica en Hoge Energie Fysica (NIKHEF), Science Park, Amsterdam, The Netherlands*
[79] *Stichting Astronomisch Onderzoek in Nederland (ASTRON), Dwingeloo, The Netherlands*
[80] *Universiteit van Amsterdam, Faculty of Science, Amsterdam, The Netherlands*
[81] *Case Western Reserve University, Cleveland, OH, USA*
[82] *Colorado School of Mines, Golden, CO, USA*
[83] *Department of Physics and Astronomy, Lehman College, City University of New York, Bronx, NY, USA*
[84] *Louisiana State University, Baton Rouge, LA, USA*
[85] *Michigan Technological University, Houghton, MI, USA*
[86] *New York University, New York, NY, USA*
[87] *Pennsylvania State University, University Park, PA, USA*
[88] *University of Chicago, Enrico Fermi Institute, Chicago, IL, USA*
[89] *University of Delaware, Department of Physics and Astronomy, Bartol Research Institute, Newark, DE, USA*

——

[a] *Fermi National Accelerator Laboratory, USA*
[b] *also at Universidade Federal de Alfenas, Poços de Caldas, Brazil*
[c] *Max-Planck-Institut für Radioastronomie, Bonn, Germany*
[d] *School of Physics and Astronomy, University of Leeds, Leeds, United Kingdom*
[e] *also at Radboud Universtiy Nijmegen, Nijmegen, The Netherlands*
[f] *Fermi National Accelerator Laboratory, Fermilab, Batavia, IL, USA*
[g] *also at Karlsruhe Institute of Technology, Karlsruhe, Germany*
[h] *Colorado State University, Fort Collins, CO, USA*
[i] *now at Hakubi Center for Advanced Research and Graduate School of Science, Kyoto University, Kyoto, Japan*
[j] *also at University of Bucharest, Physics Department, Bucharest, Romania*

* Correspondence:
spokesperson@auger.org.ar

Abstract

The Pierre Auger Observatory was built to study cosmic rays of the highest energies. It is installed in the Departments of Malargüe and San Rafael in the Province of Mendoza, Argentina. The Observatory is based on a hybrid design, comprised by two detector systems: a surface array of 1660 water Cherenkov detectors is complemented with 27 fluorescence telescopes which overlook the atmosphere above the surface array. Covering a total area in excess of 3000 km^2, it is the largest and most precise observatory of its kind. It has been in full operation for over a decade now. In this article we review the objectives and design properties of the Pierre Auger Observatory, present its performance and the main scientific results obtained so far, and we describe the Upgrade that is well underway to enhance its capabilities for the next decade of measurements.

Keywords:

cosmic rays, Pierre Auger Observatory

1. Cosmic rays and their spectrum

The discovery of cosmic rays is attributed to Viktor Hess, who in 1912 demonstrated the extraterrestrial origin of the very penetrating ionising radiation that had already been measured years before. Although it was soon established that this energetic radiation originated beyond the solar system, it was hard to discern if it was caused by photons or massive particles. It took nearly two decades of intense research and after heated debates among the top scientists in the field, it could be concluded that cosmic rays are composed of massive, charged particles, mostly high energy protons and, to a lesser degree, heavier atomic nuclei.

Cosmic ray physics was a very active field of research in the first half of the XXth century. The main breakthroughs in the dawn of particle physics were possible thanks to the existence of this cosmic radiation of very high energy. Through its study, the foundations of elementary particle physics were laid, when the positron, the muon, the pions and many other subatomic particles were discovered as by-products of interactions of cosmic rays.

At the end of the 1930s, Pierre Auger operated a number of Geiger-Müller counters in coincidence at high altitude sites in the Alps, and concluded that the penetrating radiation detected at ground level is due to so called extensive air showers (EAS), i.e., secondary particles produced by the interaction of very high energy cosmic rays with the atoms of the atmospheric air. Fig. 1 shows an artistic view of an Extensive Air Shower. In his studies, Auger concluded that the cosmic radiation must include particles with energies in excess of 10^{15} eV. Following Pierre Auger's discovery, systematic effort was invested in the study of cosmic air showers, their development and characteristics. Pioneering work by Bethe, Heitler, Greisen, Hillas, Nishimura and many others set the foundations for their description. For a historical review, see [1].

In the 1950s, surface detectors for the study of Extensive Air Showers became a widely used tool. The first measurements of energy and arrival direction of cosmic rays above 10^{15} eV were carried out in 1954 by the cosmic ray group of Bruno Rossi at MIT, using an array of 11 scintillation detectors arranged in a circle of 230 m radius. Between 1954 and 1957, the cosmic ray spectrum was explored to energies beyond 10^{18} eV with data provided by the Agassiz Station at Harvard [2]. In 1962, Volcano Ranch in Albuquerque, New Mexico, would be the first giant array to register an ultra-energetic event of 1.4×10^{20} eV [3, 4].

After the discovery of the cosmic microwave background radiation (CMBR) by Penzias and Wilson in 1964 [5], Kenneth Greisen [6] and independently Georgiy Zatsepin and Vadim Kuz'min [7] demonstrated that for protons with energies above $\sim 5 \times 10^{19}$ eV, the cross section for the interaction with the CMB photons has a sharp increase due to the Δ resonance for production of pions:

$$\begin{aligned} &\mathrm{p} + \gamma_{\mathrm{cmb}} \to \triangle^{+} \to \mathrm{n} + \pi^{+}\,, \\ &\mathrm{p} + \gamma_{\mathrm{cmb}} \to \triangle^{+} \to \mathrm{p} + \pi^{0}\,. \end{aligned} \tag{1}$$

This interaction degrades the proton energy, preventing particles with energies greater than $\sim 5 \times 10^{19}$ eV to be observed

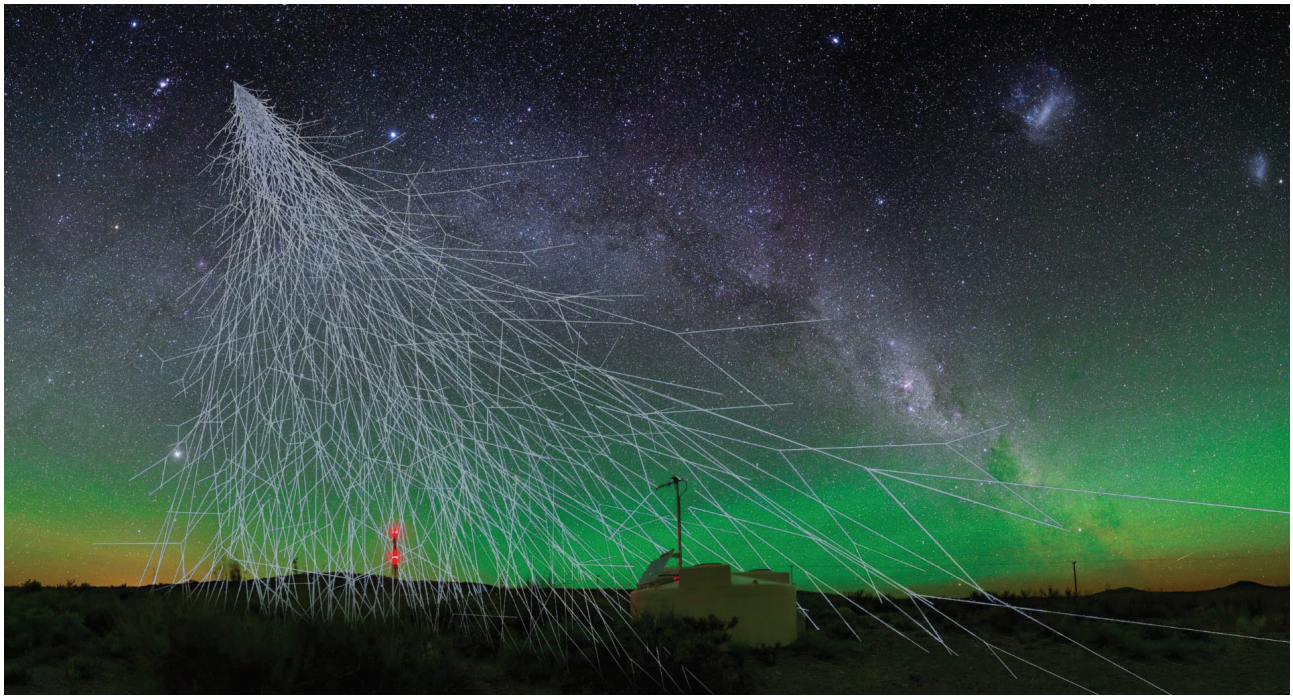

Figure 1. Artistic view of an Extensive Air Shower. Ultra high energy cosmic rays produce Extensive Air Showers with $\sim 10^{11}$ energetic secondary particles, spread over tens of km^2.

at distances larger than ~ 100 Mpc. Therefore, if cosmic rays originate at cosmological distances, the flux above this energy should be largely suppressed, giving rise to a sharp decrease in the cosmic ray energy spectrum, known as the GZK cut-off.

Similarly as for protons, for primary cosmic rays with mass number $A > 1$ the photodisintegration process comes into play, both with the microwave and the infra-red background. This leads to the ejection of one or several nucleons N from the nucleus [8, 9]. Given that the energy of the primary nuclei is shared between nucleons, the threshold energy for these processes is typically higher than for protons, but producing a similar suppression in the flux at high energies.

Therefore, a series of experiments were set up to study the upper end of the spectrum of cosmic rays. Casa Mia in USA [10], SUGAR in Australia [11], Haverah Park in England [12], Yakutsk in the USSR [13], KASCADE and Kascade-Grande in Germany [14], AGASA in Japan [15] and Fly's Eye - HiRes in the USA [16, 17, 18] recorded high energy cosmic ray events and contributed to the determination of their spectrum. In 1990, there were already a few dozens of events detected with estimated energies above the GZK cut-off, including the remarkable event with an energy of $E = 3 \times 10^{20}$ eV detected by the Fly's Eye detector in 1991 [19]. Fly's Eye was a fluorescence detector that operated from 1981 to 1993 in Utah, and was later replaced by the "High Resolution Fly's Eye" (HiRes) detector.

However, a notorious discrepancy was observed between the spectra reported by the two largest observatories, AGASA [20] and HiRes [21]. While HiRes observed a suppression at the highest energies, AGASA did not. It was conjectured that systematic errors could be the cause, as AGASA was composed of a surface array of 111 scintillator detectors and 27 muon detectors, covering some 100 km^2, while HiRes was an observatory based on the atmospheric fluorescence technique. The AGASA results seemed to contradict the expectations from the GZK suppression. If these events had an astrophysical origin, due to the GZK effect they would necessarily need to have a nearby origin (of the order of $\sim$100 Mpc). This conclusion created a tension with the expectation that in this case their arrival directions should suffer small deviations and should therefore point backwards to identifiable sources, which was not the case.

1.1. The need for a giant array

The question about the existence of the GZK cut-off was one of the main reasons for the design of a new observatory that would be able to gather enough statistics at the highest energies where the cosmic ray flux is below 1 km^{-2} century^{-1}. This piece of the cosmic ray puzzle, together with the fact that the sources of the highest energy cosmic rays had not yet been identified, were the main arguments that led to the construction of the Pierre Auger Observatory.

Due to the very low flux of cosmic rays above 10^{20} eV, vast areas need to be monitored to collect a large statistical sample. Already in 1992, James Cronin and Alan Watson had proposed the idea of building a huge array of detectors to answer the question of the origin of the cosmic rays of the highest energies, their composition, source distribution and propagation. The proposal found support and encouragement from the scientific community and, in 1995, a 6-month workshop was held at Fermilab to refine the proposal and prepare the Design Report. From the originally called "Giant Array Project", the "Pierre Auger Observatory" was born.

To get a full-sky coverage, two 3000 km^2 hybrid observatories, one in each terrestrial hemisphere, were planned, with the objective of giving a definite answer to the question of the high energy end of the cosmic ray spectrum, to individualize their sources, to study other primaries rather than nuclei (photons and neutrinos), reveal the chemical composition of primaries, and study hadronic interactions at the highest energies.

One of the key ingredients of Auger was its *hybrid detection* concept: a large-scale observatory that would combine the surface detection technique as exploited by AGASA or Haverah Park, and the fluorescence technique as pioneered by Fly's Eye and employed in HiRes. The Surface Detector (SD) is an array of detectors that are sensitive to the secondary particles of the EAS (muons, electrons, positrons and photons) as they reach the surface of the Earth, providing information on their arrival times and lateral distribution. The Fluorescence Detector (FD) consists of a set of telescopes that measure the UV light emitted by the atmospheric nitrogen which is excited by the particles of the shower as they traverse the atmosphere. The FD provides data on the longitudinal development of the EAS. While the SD is operational 24 hours per day, all year long, the FD can only operate on clear, moonless nights, with a duty cycle of $\sim$15%. The combination of information from the two detection systems enhances the reconstruction capability with respect to the individual detector reconstruction. A *"hybrid event"* is an EAS that is simultaneously detected by the FD and the SD.

Several aspects were taken into account for the choice of the observatory's location, related to the scientific goals and the construction feasibility [22]. These include the need of a site at $\sim 500-1500$ m above sea level to optimize the detection of showers produced by cosmic rays of 10^{19} eV. In addition, the communications and deployment requirements call for a relatively flat site with scarce vegetation and population.

The need to detect the faint fluorescence signals produced by the EAS requires a location with optical characteristics close to those sought for astronomical telescopes. Small elevations at the periphery of the site are required to install fluorescence telescopes above the dusty lower layers of the atmosphere. The availability of preexisting infrastructure and human resources was a requirement to guarantee a smooth construction, operation and maintenance of the observatory for at least 20 years.

A broad sky coverage was one of the important considerations for the selection of water-Cherenkov detectors (WCDs) for the surface detector array. WCDs can be relatively deep (e.g. 1.2 m at Haverah Park), while scintillators commonly used in arrays are much thinner. As such, a WCD allows the detection of much more inclined particles from the EAS. To optimise the uniformity in exposure of the sky with detectors that can reconstruct showers with a zenith angle up to 60°, two observatories are required at latitudes between 30° and 45° in both hemispheres.

2. The Pierre Auger Observatory

In 1996, after a world-wide survey for suitable sites for installation of the observatories, including Argentina, South Africa and Australia in the Southern Hemisphere, the International Collaboration agreed to install the Southern Pierre Auger Observatory in Argentina. This decision was based on the fact that Argentina could provide suitable sites, but also political, scientific and technological support. Main candidate sites in Argentina that were considered more seriously were Pampa Amarilla in the Departments of Malargüe and San Rafael in the Province of Mendoza, and the Meseta de Somuncura in Rio Negro Province [22]. In 1998 the Pampa Amarilla site was chosen, located at 35.0° – 35.3° S, 69.0° – 69.4° W and $1340-1610$ m above sea level. The observatory spans a total area of approximately 3000 km^2. It is the first hybrid observatory combining a surface array of water-Cherenkov detectors and a set of fluorescence detectors at the periphery of the array.

Although later on a decision was made to build the Northern Auger Observatory in Lamar, Colorado, USA, this plan was never fulfilled. However, the Telescope Array collaboration built a hybrid detector expanding the HiRes site in Utah, USA, and covering 762 km^2 [23].

The baseline design of the Pierre Auger Observatory [24] consists of 1600 surface detectors in a triangular grid with 1500 m between adjacent detectors. Twenty four fluorescence telescopes, located in four buildings at the periphery of the surface array, overlook the atmosphere above the array and record the fluorescence light produced by the cosmic air showers.

Additionally, an "Infill array" covering an area of 23.5 km^2 is composed of the regular array with added detectors at half-spacing between them, i.e., forming an array with 750 m distance between detectors. This denser array allows to trigger on smaller showers, caused by lower energy cosmic rays. This infill permits to lower the trigger threshold by one decade in energy and to detect with full efficiency cosmic rays down to 3×10^{17} eV. Given that at these lower energies the cosmic ray flux is considerably higher, the smaller surface is sufficient. To access even lower energies, some additional detectors have been placed at the central point of the 750 m-triangles, forming a 433 m-array. Furthermore, for timing and calibration studies, some array positions have been equipped with two or even three detectors. This brings the total number of detectors in the field to approximately 1660 units.

Also, to complement the FD, three additional fluorescence telescopes were installed to observe lower energy showers. These instruments are dubbed "HEAT", which stands for High Elevation Atmospheric Telescopes. As the maximum development of lower energy showers occurs higher in the atmosphere, the HEAT telescopes have a field of view with an elevation between 30° and 60°.

A full, detailed description of the Pierre Auger Observatory can be found in [24]. Fig. 2 shows one of the WCDs of the SD in front of the Los Leones FD building. Fig. 3 shows the layout of the Observatory.

Figure 2. One surface detector deployed in the field, in the background one of the FD buildings and the communications tower.

The construction of Auger began in 2001 with an Engineering Array consisting of two fluorescence telescopes and 32 WCDs deployed within the fields of view of the two telescopes. The construction and operation of the Engineering Array allowed to optimise the techniques related to the production and deployment of the detector components, the trigger algorithms, the data acquisition, monitoring software and telecommunications for both detection systems [25]. In 2004, the project entered into the production phase and in 2008 the construction of the Observatory was concluded.

2.1. The surface detector array

The principle of operation of the SD stations [24, 26] is based on the Cherenkov light emission in water. When relativistic secondary particles from an air shower propagate in water, they produce Cherenkov light. This is true for charged particles such as electrons, positrons and muons of the air shower when their speed exceeds the speed of light in water. Also, when high energy photons interact with the water, they produce electron-positron pairs which can also be detected by their Cherenkov emission.

Each WCD consists of a volume of 12,000 litres of ultra-pure water contained in a liner within a rotomolded polyethylene tank. The tanks are 3.6 m in diameter and 1.5 m high. The liner is black on the outside, for light tightness, and covered with a highly reflective and diffusive inner surface, provided by a Tyvek film, to distribute uniformly the Cherenkov light within the water volume.

The ultra-pure water (resistivity above 12 MΩ-cm) is produced in a water purification plant that was installed in the Auger Central Station in Malargüe. Once deployed at their correct positions in the field, the tanks are filled with ultra-pure water transported in clean specialized transport tanks. Because of its high purity, the water maintains its clarity without significant degradation during the lifetime of the observatory. Periodic bacteriological tests have indicated that the ultra-pure water and the environment free of light and organic residues does not support bacterial growth which could lead to reduced water clarity.

The SD stations are completely autonomous. Electrical power is provided by two 55 Wp (Watt-peak) solar panels and a pair of 12V, 105 Ah batteries, which provide a 24 V power system. Batteries are charged through a commercial charge controller. The electronics assembly at each SD station possesses a Tank Power Control Board (TPCB) which monitors the power system operation. The batteries are accommodated in a rotationally molded polyethylene battery box, protected from direct sunlight at the southern side of the tank. The solar panels are mounted on aluminium brackets, which also support a mast. Antennas for radio communications and GPS reception are mounted at the top of this mast.

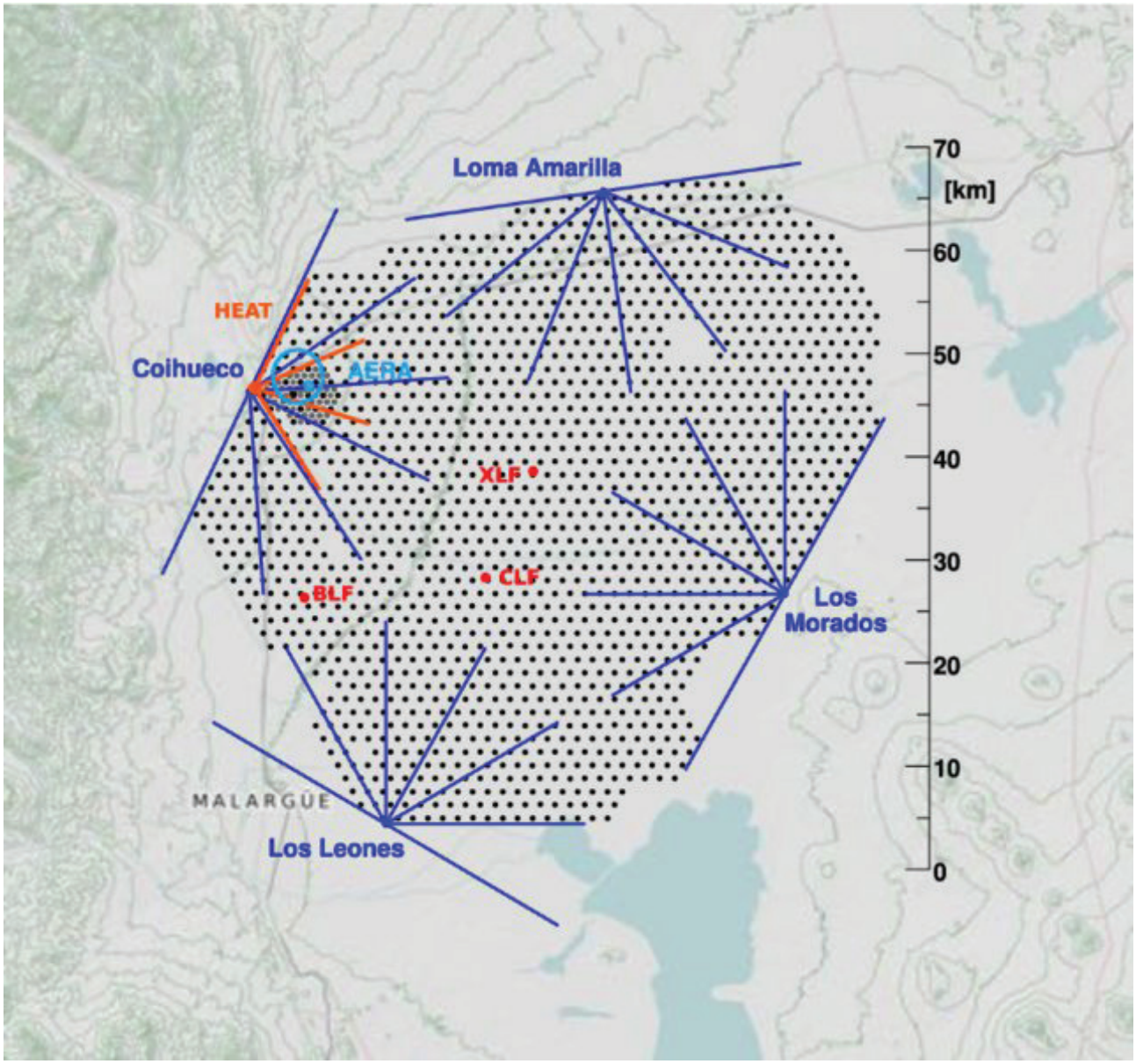

Figure 3. The layout of the Pierre Auger Observatory. Each black dot represents a WCD. The scale can also be inferred from the distance of 1500 m between adjacent detectors. Lines from the FD buildings represent the field of view of each of the fluorescence telescopes.

2.2. SD electronics

The Cherenkov light produced in the detector is collected by three 9-inch photomultiplier tubes (PMTs) which view the water volume from above, through three window domes integrated to the liner. Each PMT has two outputs. An AC coupled anode signal is provided. In addition, the signal at the last dynode is amplified and inverted by the PMT base electronics to provide a signal with 32 times the charge gain of the anode.

Six identical channels of electronics are provided to digitize the anode and amplified dynode signals from each of the PMTs. The analog signals from the PMTs are fed to Analog Devices AD9203 10 bit 40 MHz semi-flash analog to digital converters (ADCs), corresponding to time bins of 25 ns for the signals. The use of two 10 bit ADCs with a gain difference of 32 extends the dynamic range of the system to 15 bits. The maximum signal recorded before saturation corresponds to

about 650 times the peak current from a vertical muon traversing the tank, which corresponds to the signal from a 10^{20} eV cosmic ray at about 500 m from the shower core.

Each SD station contains a GPS receiver with its corresponding antenna mounted at the top of the communications mast for event timing and communication synchronization. The absolute timing of the signals in individual WCDs is relevant for reconstructing the shower front and computing the arrival directions of the incoming cosmic rays. The time-tagging system allows to adjust the ADC data to GPS time within 10 ns RMS.

Communications with the Central Station is done through a WLAN customs radio network operating in the 902-928 MHz band. Four concentrators located at the FD buildings collect the data from the field and transfer it through a dedicated microwave link to the Central Station. This microwave link also transports the FD data. Communications with the individual WCDs is bidirectional, so that the full trigger information can be requested from the WCD by the Central Data Acquisition System (CDAS) on demand, and software updates and reset commands can be sent to the individual detectors.

2.3. SD trigger, calibration and event reconstruction

The SD trigger system is hierarchical. The first two triggers (T1 and T2) are at the local level of each WCD, whereas the third level trigger, T3, occurs at a global level [27]. The first level trigger, T1, has different independent modes. It triggers either when all three PMT signals exceed a threshold value, or on lower signals extended in time. The second trigger level, called T2, decreases the global rate of the T1 trigger down to about 23 Hz. All T2s send their timestamp to CDAS for the global trigger (T3) determination.

To identify real EAS, a coincident T2 trigger in adjacent WCDs is required. For example, at the highest energies, above 10^{19} eV, the footprint of the air shower on the ground extends over more than 25 km^2. To apply the main trigger condition, the central trigger processor is used to identify groups of locally triggered stations clustered in time and space. At least three stations in a compact configuration and in a compatible time window are required to form a T3 trigger. With the arrangements described above, the total T3 trigger rate of the observatory is presently of the order of 0.1 Hz and about 3 million SD events are recorded yearly. The T3 trigger is the shower trigger that results in the recording of 768 samples (19.2 μs) of the six signals (anode and last dynode signal from each of the three PMTs).

The SD array has full trigger efficiency for events of energy above 2.5×10^{18} eV. The Infill array allows to reduce the threshold for full acceptance by more than a full order of magnitude in energy.

Calibration of the SD stations is performed during routine operation of the detector. The total bandwidth available from each SD station to the central station requires that the calibration be done by the local electronics. Also, the remoteness of the detectors requires the calibration procedure to be robust.

The Cherenkov light recorded by a surface detector is measured in units of the signal produced by a muon traversing the tank on a vertical trajectory through its centre. This unit is termed the "vertical equivalent muon" (VEM). The goal of the surface detector calibration is to measure the value of 1 VEM in hardware units (i.e., in integrated FADC channels). The conversion to units of VEM is done both to provide a common reference level between tanks and to calibrate against the detector simulations.

For this purpose, each station has a trigger mode which allows to record small signals, which are mostly due to single muons and other single particles traversing the detector. A histogram of the total charge produced by these signals has a characteristic peak which is related to the total signal deposited by omnidirectional atmospheric muons. The relation between this histogram peak and the signal produced by a single, through-going vertical muon can be established from measurements with muon hodoscopes. Ref.[28] describes in detail the calibration method of the surface detector.

To ensure good quality of the data used for physics analysis, two additional off-line "triggers" are implemented. One of them, called T4, selects real showers and discards random coincidences of nearby detectors which have triggered on low energy showers. This trigger is mainly based on a coincidence between adjacent detector stations within the propagation time of the shower front. Additionally, a fiducial cut is applied to preserve events whose shower core is within an area well enclosed by functioning detectors. This cut is required both to make sure that the reconstruction is not biased and to define a precise volume for acceptance calculations.

The reconstruction of the energy and the arrival direction of the cosmic rays producing air showers that have triggered the surface detector array is based on the signal sizes and start times of the traces registered by individual stations. For a recent summary, see [29]. The total signal recorded by the WCDs, which is a measure of the total energy transferred to Cherenkov light inside the detector, is converted into units of VEM. Reconstruction of showers with the SD requires fitting the signals observed in each of the triggered detectors to a lateral distribution function, and the arrival times to a shower front shape. This allows to reconstruct the impact point of the shower core, the azimuthal and zenith angle of the shower axis, and the lateral spread of the signal as a function of the distance to the shower axis. From the information on the lateral spread of the shower, the signal expected at a reference distance of 1000 m from the shower axis, $S(1000)$, can be interpolated. The reference distance of 1000 m is chosen because it minimises the fluctuations in the expected signal for the array geometry with a spacing of 1500 m between adjacent detectors. However, this value of $S(1000)$ needs to be corrected for the dependence of the atmospheric attenuation with zenith angle. For this correction, a Constant Intensity Cut method is used, which is based on the fact that the flux of cosmic rays above a certain energy is independent of the arrival zenith angle. A correction factor is applied to the $S(1000)$ as a function of zenith angle and energy, so that the fluxes are

equalized in all zenith angle bins. The zenith angle-corrected $S(1000)$, normalized to its value at the median angle of 38° is called S_{38°. The assignment of the absolute energy scale to S_{38° is based on the hybrid data acquired in conjunction with the FD and will be mentioned in the following section.

The accuracy in the evaluation of the arrival direction of the shower depends on the start times of the individual stations. Timing precision with the WCDs is of 10 ns. The overall angular reconstruction accuracy of the WCDs can be derived by means of simulations, and at the highest energies it results to be better than 1° for all simulated primary masses and shower axis directions.

Fig. 4 shows a typical event recorded by the Auger SD in 2020.

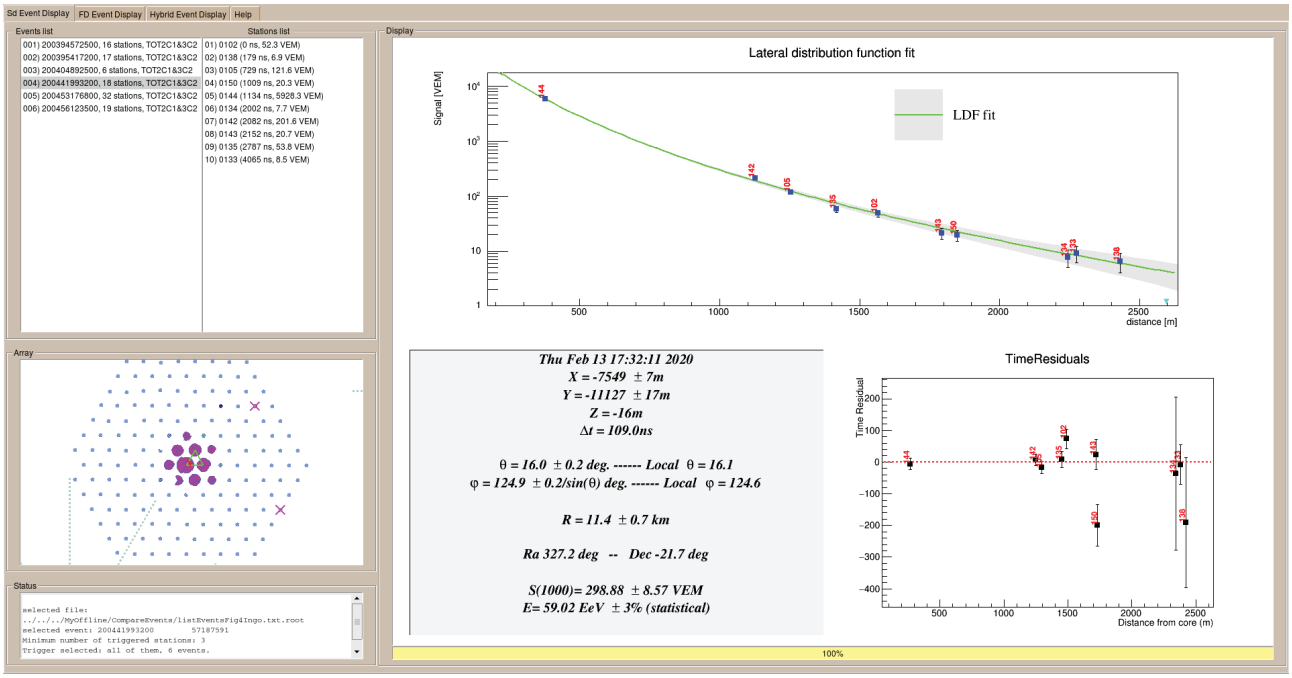

Figure 4. A typical event recorded with the Surface Detector Array, as visualized with the Auger Event Display. The lateral distribution of signals in the intervening SD is shown as a function of the distance to the shower core, together with the fitted lateral distribution function.

2.4. The luorescence telescopes

The 24 fluorescence telescopes [24, 30] are located in four buildings at the periphery of the SD array, on small elevations named Los Leones, Coihueco, Loma Amarilla and Los Morados. Each site hosts six telescopes, in six independent bays within a building with controlled climate. Each telescope has a field of view from 1° to 31° in elevation and covering 30° in azimuth.

Nitrogen fluorescence light, emitted isotropically by an air shower, enters through a circular diaphragm of 1.1 m radius covered with a filter glass window which only allows the passage of UV light, to reduce the background light. The filter also serves as a window over the aperture. The telescopes are based on Schmidt optics to reduce the coma aberration of large optical systems. A shutter system and fail-safe curtains protect the telescope when not in operation or when excessive outside light or weather effects are detected. A simplified annular lens to correct spherical aberration and eliminate coma aberration is mounted in the outer part of the aperture.

The fluorescence light is collected by a segmented spherical mirror of 3400 mm radius of curvature onto a spherical focal surface with radius of curvature 1700 mm. The primary mirror has an area of 13 m^2. The camera consists of an array of 440 photomultiplier tubes of 40 mm diameter each. These are arranged in a matrix of 22 rows by 20 columns. The field of view of each pixel corresponds to an angular size of 1.5°.

The FD electronics must provide a large dynamic range and strong background rejection, while accepting any physically plausible air shower. Moreover, the electronics includes capabilities for antialias filtering, digitizing, and storing signals from the PMTs. The signal is shaped and digitized in the front-end electronics (FE) unit, where threshold and geometry triggers are also generated. Analog boards in the FE unit are designed to handle the large dynamic range required for air fluorescence measurements; this means a range of 15 bits and 100 ns timing.

As the PMT data are processed, they are passed through a flexible three-stage trigger system implemented in firmware and software. The trigger rate of each pixel in a camera (first level trigger) is kept around 100 Hz by adjusting the pixel threshold level. The algorithm of the second level trigger searches for track segments at least five pixels in length within a camera. The typical trigger rate per camera fluctuates between 0.1 and 10 Hz. The third level trigger is a software algorithm

designed to clean the air shower data stream of noise events that survive the low-level hardware triggers. It is optimized for the fast rejection of triggers caused by lightning, triggers caused by cosmic ray muon impacts on the camera and randomly triggered pixels. Data from an event that survives all three trigger levels is merged between all the telescopes and generates a hybrid trigger (FD-T3) for the surface array. The event rate is about 0.012 Hz per site for the 24 baseline telescopes.

It should be noticed that unlike the SD, for the FD the energy threshold for detection depends on the distance and the relative geometry of the shower with respect to the FD building.

The precise reconstruction of air shower longitudinal profiles requires the conversion of an ADC count to a light flux for each pixel that receives a portion of the signal from a shower. To this end, the absolute calibration of the detector response is essential. In the first years of operation, a calibrated, large diameter, drum-shaped light source provided an absolute, end-to-end calibration for each pixel of the fluorescence telescopes, with independent verification for some pixels by atmospheric Rayleigh scattering from vertical laser pulses. For these absolute methods, the flux of photons on the telescope aperture is independently measured. The effects of diaphragm area projection, optical filter transmittance, mirror reflectivity, pixel light collection efficiency and area, cathode quantum efficiency, PMT gain, preamplifier and amplifier gains, and digital conversion are all included in the end-to-end calibration procedure. Presently, a new calibration method is being implemented, based on a calibrated point-like UV light source, which is movable and scans all the front surface of the aperture of the telescopes.

Hybrid events are those recorded simultaneously by FD and SD systems. Hybrid events allow a very precise timing of arrival of the shower, which is required for a precise geometric reconstruction. Events that trigger three or more SDs, so that an independent reconstruction can be made with SD alone, are named "Golden hybrid". These are of particular importance for the energy calibration of the SD events.

2.5. Energy calibration

Once the geometry of the shower is known, the light collected at the aperture as a function of time can be converted to the energy deposited by the shower as a function of the traversed atmospheric depth X. For this purpose, the light attenuation from the shower to the detector needs to be accounted for, and all contributing light sources need to be disentangled: fluorescence light, direct and scattered Cherenkov light as well as multiply scattered light. The proportionality between the fluorescence intensity and the energy deposit is given by the fluorescence yield. A good knowledge of its absolute value as well as its dependence on wavelength, temperature, pressure and humidity is essential to reconstruct the longitudinal profile.

The full longitudinal profile of the energy deposit and its maximum $(dE/dX)_{\max}$ at depth $X = X_{\max}$ are estimated by fitting an asymmetric bell-shaped Gaisser–Hillas function to the time profile of photoelectrons detected in the PMTs of the FD cameras. For this purpose, a log-likelihood fit is used in which the number of photoelectrons detected by the PMTs of the FD cameras is compared to the expectation from the Gaisser-Hillas function after folding it with the light yield, atmospheric transmission, lateral distributions and detector response.

Finally, the calorimetric energy of the shower is obtained by integrating over the total longitudinal profile and the total energy is estimated by correcting for the "invisible energy" carried away by neutrinos and high energy muons.

To assign the energy to the showers detected with the SD, the "golden hybrid" events are used for cross-calibration. High-quality hybrid events with reconstructed zenith angles less than 60° are used to relate the shower size from SD to the almost-calorimetric measurement of the shower energy from FD, $E_{\rm FD}$. For the FD part of the event, we require an accurate fit of the longitudinal profile. Furthermore, the depth of the shower maximum $X_{\max}$ must be contained within the telescope field-of-view and measured with an accuracy better than 40 g/cm^2. The uncertainty on the reconstructed $E_{\rm FD}$ is required to be less than 18%. The final criteria for defining the calibration data sample include a selection of data with clear atmospheric conditions.

The final step in the calibration analysis leads to a relation between S_{38° and $E_{\rm FD}$. The correlation between the two variables is obtained from a maximum likelihood method which takes into account the evolution of uncertainties with energy, as well as event migrations due to the finite energy resolution of the SD. The relation between S_{38° and $E_{\rm FD}$ is well described by a single power law function, as shown in Fig. 5 [34].

Systematic uncertainties in the energy scale add up to 14%, the major contribution arising from the absolute calibration of the telescopes, with a value of 9.9%, the other contributions arising from fluorescence yield, atmosphere, profile reconstruction, estimation of invisible energy and energy scale stability.

The recorded dataset extends up to larger angles approaching 90°. For the inclined events, with zenith angles larger than 60°, we employ a different reconstruction method, yielding to the energy estimator N_{19}, the relative muon content with respect to simulated proton showers at 10^{18} eV. The energy range of full efficiency of the surface detector has been extended down to 3×10^{16} eV using the events recorded by the infill array. For infill events, the analogous energy estimator is S_{35°.

2.6. Complementary equipment and infrastructure

Other vital components and equipment relevant to the functioning of the Observatory are described in [24] and in references therein. These include the full communications system, the Central Data Acquisition System (CDAS), the data handling and storing, the monitoring tools and the Offline framework for data processing and analysis.

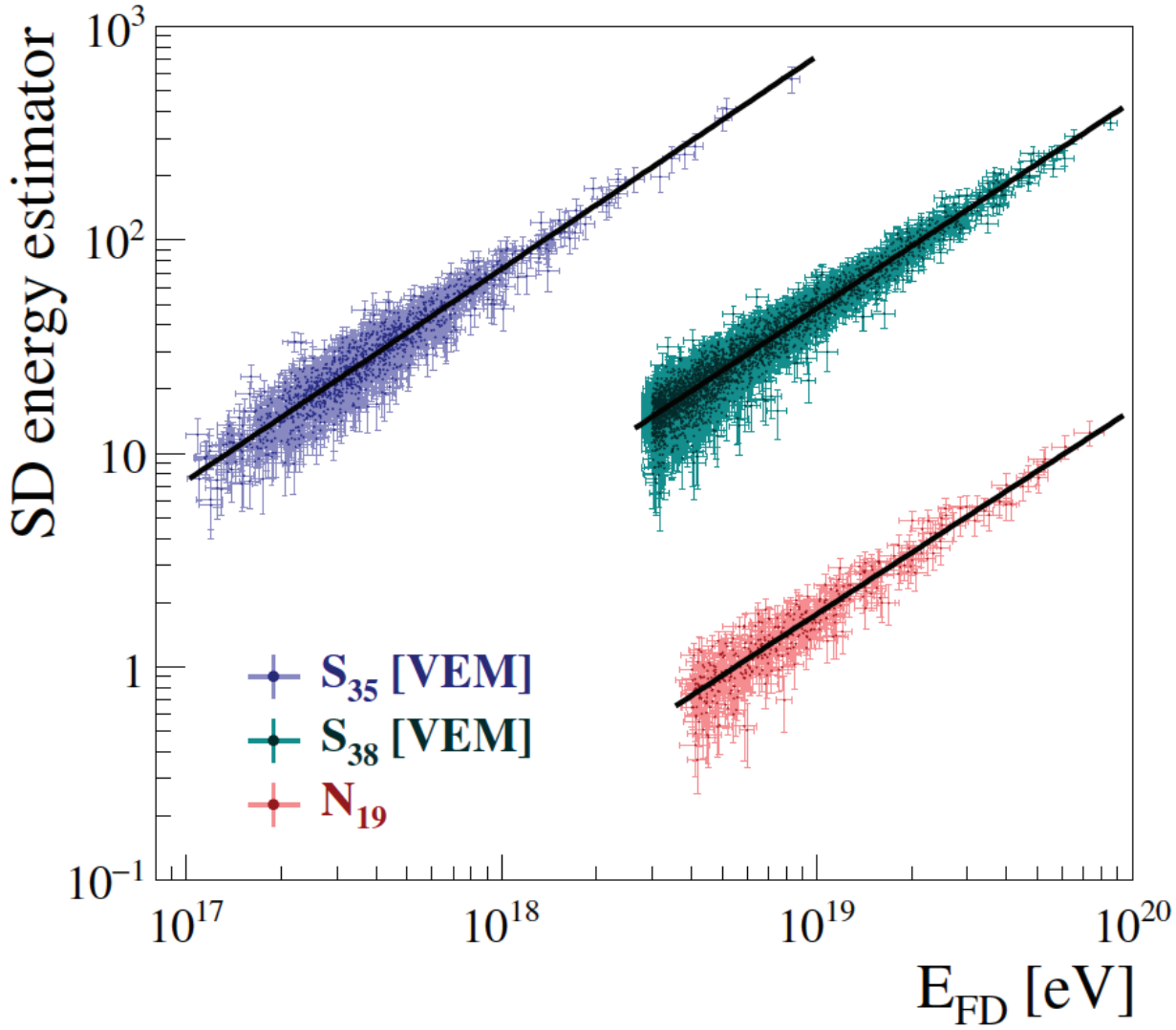

Figure 5. Relation between the SD energy estimator S_{38° and the calorimetric FD energy E_{FD} for good quality golden hybrid events. Also shown is the relation with the energy estimator S_{35° for lower energy showers detected with the 750 m infill array, and the energy estimator N_{19} for inclined showers.

The Pierre Auger Observatory runs an extensive atmospheric monitoring program for characterizing the atmosphere,both to understand the light absorption for FD and to obtain the input parameters for the weather correction of SD events (pressure, temperature, air density).

The knowledge of the vertical atmospheric profile is of paramount importance for understanding the shape of the longitudinal shower development in the atmosphere. In the first years of operation of the Observatory, radiosondes were launched from the observatory site to measure air properties as a function of height. This information was used to calibrate the atmosphere to the information provided by the Global Data Assimilation System (GDAS), which is now used as input for shower reconstructions.

The observatory additionally uses five ground-based weather stations to monitor the ground-level pressure, temperature, humidity, and wind velocity with a time resolution of 5 min.

The atmospheric monitoring includes two laser facilities, dubbed CLF and XLF, installed at 12km from each other in the centre of the array, from which vertical UV laser pulses are fired. This laser light is registered by the FD telescopes in order to determine the light attenuation in the atmosphere. At the CLF station there is also a Raman LIDAR system, which is used to make three measurements of the vertical aerosol profile each night: before, during, and after the FD observations.

LIDARs located near the FD buildings record the back-scattered light in order to determine cloud levels and aerosol layers. Cloud monitoring cameras, photometric robotic telescopes for star tracking, and aerosol samplers complete the available equipment.

3. Main scienti ic results

3.1. Spectrum

The Pierre Auger Observatory allows to determine the spectrum of Ultra-High-Energy cosmic rays at the highest energies with unprecedented precision.

The regular surface detector array (SD array with a spacing of 1500 m between adjacent detectors), after calibration with the hybrid data acquired together with the FDs as explained before, allows to reconstruct the spectrum spanning the energy interval starting from 2.5×10^{18} eV up to the highest energies. At the lower limit, the SD array still has full acceptance, therefore the determination of the aperture is based only on the array geometry and the uptime of the WCDs. The most recent dataset contains more than 215,000 events with reconstructed zenith angle $\theta < 60^{\circ}$, corresponding to an exposure of (60,400 ± 1,810) km^2 sr yr. The addition of "inclined" events with $60^{\circ} < \theta < 80^{\circ}$ allows to increase the exposure by roughly 30%.

The Pierre Auger Observatory has capabilities to extend the spectrum below the energy range described above (see [31] and references therein). To determine the spectrum below the full aperture of the 1500 m SD, hybrid events recorded by the FD in combination with one of the SD, allow to go down in energy to $E > 10^{18}$ eV. Even lower energies, $E > 10^{17}$ eV, can be achieved with the SD infill, where WCDs have a spacing of 750 m. Using events detected with the HEAT telescopes, which are dominated by Cherenkov light, allows to study the spectrum at energies as low as $E > 10^{16.5}$ eV [33, 34].

The full, combined spectrum, is depicted in Fig. 6. Given that the flux is a steep function of the energy, is is customary to plot the flux multiplied by a power of the energy (in this case, E^3), to highlight the features of the spectrum.

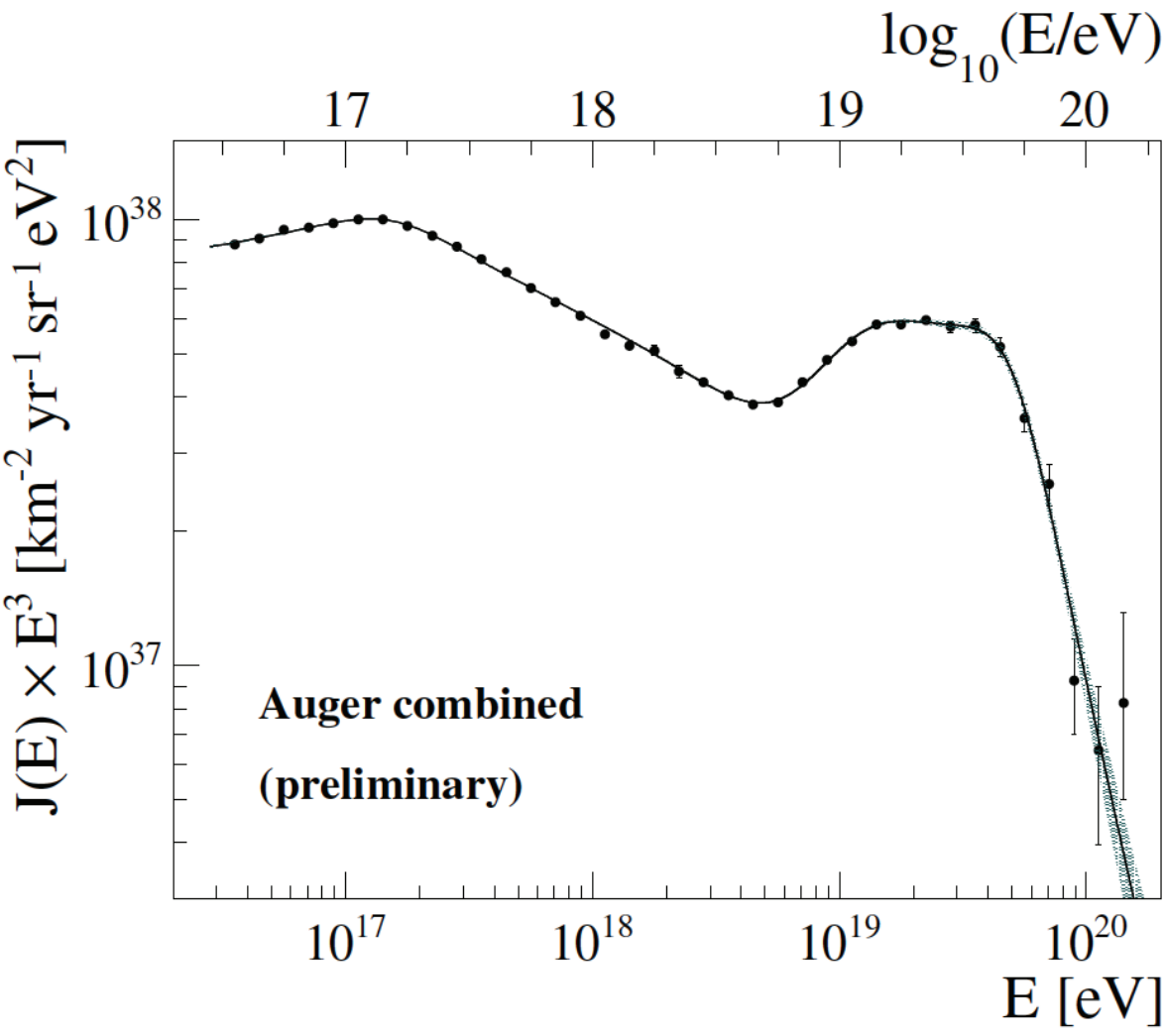

Figure 6. The combined spectrum of the Pierre Auger Observatory, multiplied by E^3 to emphasize its features.

The spectrum above 2.5×10^{18} eV can be well fitted with a broken power law in four intervals, as described in [32]. In each interval, the functional form is assumed to be $dN/dE \sim E^{-\gamma}$, where γ is the spectral index in the corresponding

interval. The high-energy suppression has been clearly identified above an energy of $E_{34} = (46 \pm 3 \pm 6) \times 10^{18}$ eV with a slope given by $\gamma_4 = 5.1 \pm 0.3 \pm 0.1$, confirming with the highest precision the previous reports of the strong attenuation of the flux at these energies [21, 35, 36]. Determining whether this suppression is a GZK-like effect arising from the propagation of cosmic rays in the intergalactic medium, or due to an exhaustion of the injection power of the astrophysical sources is as yet not clear. To find an answer to this question is one of the main goals of the Upgrade, described further on in this review.

The "ankle" is a known spectral feature described by a rollover at $E_{12} = (5.0 \pm 0.1 \pm 0.8) \times 10^{18}$ eV, marking a hardening of the spectrum from $\gamma_1 = 3.29 \pm 0.02 \pm 0.10$ to $\gamma_2 = 2.51 \pm 0.03 \pm 0.05$. This ankle has been widely reported in the literature [21, 37, 38]. Different possible explanations have been suggested for this feature, e.g. the transition from a galactic to an extragalactic origin of cosmic rays, or a dip due to the contribution of e^+- e^- pair production resulting from cosmic ray proton interactions with the cosmic microwave background. The Auger measurements favor instead the interpretation that it results from the transition from an extragalactic component dominated by light elements for lower energies to one with intermediate and heavier masses at higher energies.

A novel feature that also has to be accounted for in an integrated description of the spectrum is the break at $E_{23} = (13 \pm 1 \pm 2) \times 10^{18}$ eV, where the spectrum softens from γ_2 to $\gamma_3 = 3.05 \pm 0.05 \pm 0.10$.

At lower energies, the spectrum shows a clear inflection point corresponding to the so-called "second knee" around 10^{17} eV, which is normally explained as related to the maximum energy at which the Fe group galactic cosmic rays can be accelerated.

3.2. Composition

The determination of the mass composition of the primary cosmic rays is a major experimental challenge. The most precise and straightforward determination is based on the analysis of the atmospheric depth at which the shower exhibits its maximum development, X_{max}. Showers initiated by protons and other light primaries develop deeper in the atmosphere, leading to larger values of X_{max}. Also, the number of muons N_μ in the shower is a good proxy for studying the composition: showers from light primaries contain less muons than showers initiated by heavier nuclei, as will be described in Section 4. From a simple superposition model (see, e.g., [39]), the $\langle X_{max} \rangle$ of the showers varies linearly with $< \ln A >$, being A the atomic mass of the primary, and it is therefore a sensitive parameter for mass composition. Although more complex to interpret for mixed compositions, the behaviour of the fluctuations of X_{max}, i.e., $\sigma(X_{max})$, also gives information of the primary mass.

The direct measurement of X_{max} can only be achieved with the fluorescence technique. The HEAT telescopes provide the adequate field of view to record the low energy showers that develop higher in the atmosphere.

Comparing X_{max} and its standard deviation to results from simulations based on different hadronic interaction models allows us to interpret its evolution with energy. The latest results can be found in [34, 33] and are displayed in Fig. 7. Based on 47,000 hybrid events, this analysis shows a trend towards lighter composition as energy increases up to 2×10^{18} eV and then to a heavier composition at higher energies.

The elongation rate is defined as the variation of the average X_{max} with energy, $d\langle X_{max} \rangle / d \log E$. The values obtained are 77 ± 2 (stat) g cm^{-2}/decade below $E_0 = 10^{18.32 \pm 0.03}$ eV and 26 ± 2 (stat) g cm^{-2}/decade above this energy. This result suggests a composition getting lighter up to E_0 and going towards intermediate-heavy masses above it. As can be seen in the comparison to results from simulations, the observed elongation rate is not compatible with a constant composition, which would require instead an elongation rate of ~ 60 g cm^{-2}/decade in the whole energy range. The results reported for $\sigma(X_{max})$ at the highest energies strongly suggest a pure and heavy composition, while in the lower energy range they are compatible with both a light or mixed composition.

Other more indirect methods for the determination of the primary mass have also been explored [40]. Although not so precise, given the higher statistics they allow to measure composition in a broader energy interval.

Any integral astrophysical interpretation of the Auger data has to describe both the spectral features and the composition evolution with energy. A combined fit of spectrum, mass composition and its fluctuations has been described in [32, 41]. The fit has been performed for energies above 5×10^{18} eV, i.e. the region above the "ankle" of the all-particle spectrum. The astrophysical model consists of identical sources uniformly distributed in comoving volume, where nuclei are accelerated through a rigidity-dependent mechanism. The fit results suggest that the sources are characterized by relatively low maximum rigidity of the particles at the acceleration site, hard spectra and mixed chemical composition, with heavier elements becoming dominant as the energy increases. The steepening of the spectrum at $\sim 10^{19}$ eV suggests the interplay between the flux contributions of the helium and carbon-nitrogen-oxygen components injected at the source with their distinct cut-off energies, combined with photodisintegration effects during the propagation. However, uncertainties about physical quantities relevant to cosmic ray propagation and shower development have a non-negligible impact on the fit results. To make progress along these lines of research, a more precise determination of the mass composition on an event-by-event basis is required, with high statistics to reach the upper end of the spectrum where events are scarce. This program is pursued with the Upgrade of the Auger Observatory described in Section 4.

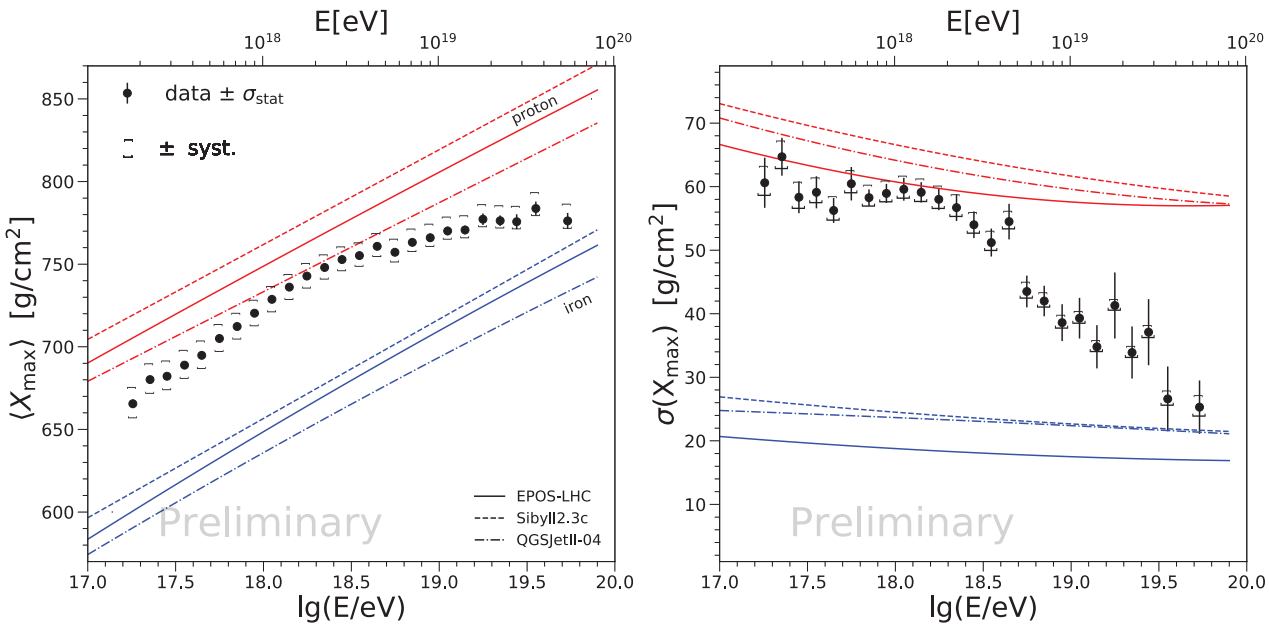

Figure 7. X_{max} (left) and $\sigma(X_{max})$ (right) as a function of primary energy, and comparison to the expectations from simulated showers with different hadronic models for proton (red) and iron (blue) primaries.

3.3. Arrival direction anisotropies

A basic objective in the study of cosmic rays and in the quest to determine their origin is the search for anisotropies in the arrival directions. These anisotropies might manifest themselves at different angular scales and energy ranges.

At higher energies, cosmic rays are expected to come from nearby, as the flux from far away sources is suppressed due to energy losses suffered during propagation. On the other hand, the particles with larger rigidity are expected to suffer smaller deflections by the galactic and intergalactic magnetic fields. Therefore, at the highest energies, tracing backwards the arrival directions should hint to the sources, or at least reveal anisotropies correlated with the directions of the sources. Searches for anisotropies on small and intermediate angular scales have been performed by exploiting 15 years of data, reaching an unprecedented exposure of ∼100,000 km^2 sr yr in a declination range between -90° and $+45^\circ$. One strategy for searching for anisotropies is based on scanning the sky for an excess in the flux of particles in different angular scale windows. The advantage of this search is that it is model independent and does not require any assumption on the possible sources. This search was performed over the whole field of view, in a wide energy threshold range $E_{thr} = 32\text{-}80 \times 10^{18}$ eV, using a 1×10^{18} eV step and scanning circular regions of radius Ψ from 1° to 30° in steps of 1°. The most significant excess was found for $E > 3.8 \times 10^{19}$ eV in an angular window of 27° centered in the direction ($\alpha = 202^\circ$, $\delta = -45^\circ$) [34]. This direction corresponds to a region densely populated with extragalactic objects, among which is Centaurus A, our closest radio galaxy. Indeed, the excess of events in its direction, already pointed out in the past [42], reached a one-sided post-trial significance of 3.9σ for energies above $E_{thr} = 3.7 \times 10^{19}$ eV and for $\Psi = 28^\circ$.

The arrival directions of ultrahigh energy cosmic rays were also studied by searching for correlations with the distribution of nearby extragalactic matter. This has been modelled by using different catalogs of possible sources up to a distance of ∼250 Mpc. In [34, 42], the following sources were considered: (a) a sample of 32 starburst galaxies (SBGs) selected based on their continuum emission at 1.4 GHz, used as a proxy for their UHECR flux; (b) a selection of γAGNs from the 3FHL catalog, weighting the sources with the integral flux from 10 GeV to 1 TeV; (c) the 2MRS catalog of nearby matter farther than 1 Mpc; (d) a selection of Swift-BAT radio-loud and radio-quiet AGNs.

In this analysis, we exploited the source directions and also the possible scenarios for the relative UHECR fluxes from source candidates provided by the observations from Fermi-LAT. Furthermore, our current knowledge of the cosmic ray composition could be used to evaluate the attenuation in intensity due to the energy losses during propagation. A likelihood ratio analysis allowed us to evaluate the smearing angle and the fraction of anisotropic cosmic rays for each case. The highest significance is obtained for the case of SBGs, where we found an anisotropic fraction of (11±5)% of events with energy above 3.8×10^{19} eV in a smearing angle of 15°. Note that the attenuation of particles in the case of the nearby SBGs is much less important than for more distant blazars. After penalization for the scanning in energy, the significance of the correlation results to be 4.5σ.

In 2017, the Pierre Auger Collaboration announced the observation of a large-scale anisotropy in the arrival directions of cosmic rays above 8×10^{18} eV [43]. This analysis was extended in [44] to a broader energy range, using about 15 years of data. For energies above 4×10^{18} eV, data from the fully efficient 1500 m SD array were used, reaching a total exposure of 92,500 and 60,700 km^2 sr yr for events with $\theta \leq 80^\circ$ and $\theta \leq 60^\circ$ respectively. Under the assumption that

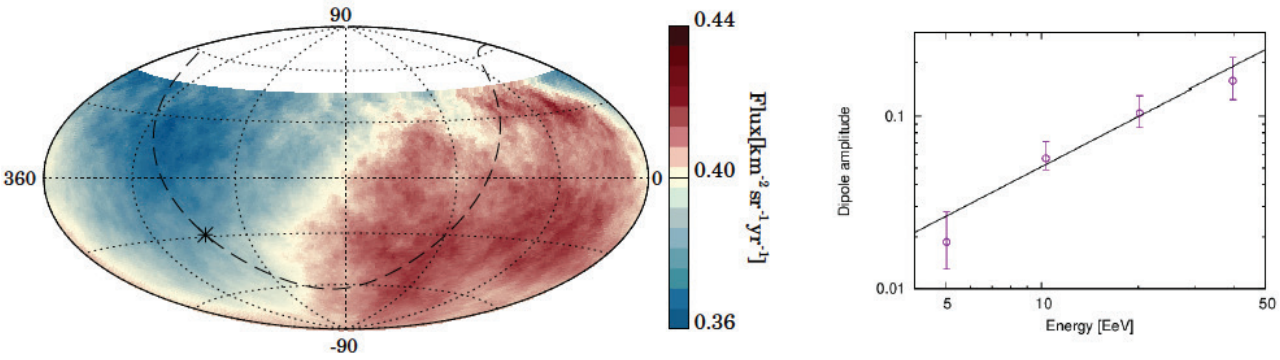

Figure 8. Left: Map of the flux of cosmic rays above 8×10^{18} eV, in equatorial coordinates. The Galactic plane and the Galactic centre are indicated by a dashed line and a star, respectively. The flux is averaged on windows of 45° radius. Right: Energy dependence of the dipolar amplitude measured in four energy bins above 4×10^{18} eV.

higher multipoles are negligible, we found a total dipolar amplitude for $E \leq 8 \times 10^{18}$ eV of $d = 0.066 \pm 0.012$, with a 6σ significance, pointing $\sim 125^{\circ}$ away from the direction of the Galactic centre, as shown in Fig. 8. This result strongly indicates an extragalactic origin of the modulation.

3.4. Search for neutrinos and photons

The Pierre Auger Observatory possesses the capability of recording and identifying extensive air showers initiated by neutrinos or photons. The interaction of UHECRs with the radiation background during their propagation is expected to produce a diffuse flux of neutrinos and photons, caused by the decay of charged and neutral pions respectively, produced in the photon-nucleon collisions. The resulting neutrino and photon fluxes depend critically on the cosmological evolution of the cosmic ray sources, and on their composition and injection spectra [45].

In FD, high energy photons can be identified because they are more penetrating than nuclei, therefore producing a much larger X_{max}. With SD, photon showers are characterised by a very low muonic content in the shower and by its steeper lateral distribution.

The search for neutrinos is based on the study of horizontal showers. When initiated by nuclei, very inclined showers traverse a large amount of air, thus producing a shower development in which the electromagnetic component has been very much attenuated, therefore the shower is dominated by energetic muons. Contrarily, showers initiated by neutrinos are expected to develop much deeper in the atmosphere, therefore still containing a large electromagnetic component when reaching the SD. Also, Earth-skimming tau-neutrinos can give rise to upwards pointing showers that are a characteristic signature for neutrinos. It turns out that Auger has an aperture for the detection of neutrinos at the highest energies that is comparable to that of other neutrino observatories.

Photons and neutrinos propagate through space in lightlike paths, therefore no time delays are expected with respect to gamma or radio emissions. This capacity positions the Auger Observatory as an important partner in multimessenger astronomy.

Present Auger limits on photon and neutrino fluxes at ultra-high energy can be found in [46, 47]. The upper limits on the photon flux have been relevant to exclude some "top-down" source scenarios, such as those in which ultrahigh energy cosmic rays originate from the decay of super-heavy particles. The limits above 10^{18} eV energies also constrain the most optimistic models of photon production from the interaction of protons with the Cosmic Microwave Background. Present bounds on neutrinos and photons will be further improved as statistics increases with increased aperture.

3.5. Additional results

3.5.1. Hadronic interactions

Collisions of cosmic ray protons of energies of 10^{20} eV with air nuclei have a centre of mass energy $\sqrt{s}$ larger than 400 TeV, which is more than 30 times beyond the reach of human-made accelerators. Therefore, the observation of the development of showers in the atmosphere can provide valuable information about high-energy hadronic interactions in an energy range not yet accessible with particle colliders. The shower development depends on many different features of the hadronic interactions. In particular, by measuring the depth of maximum development of the EAS, X_{max}, we obtain information about the cross-section of the first interaction. The determination of the muonic component at the ground is more sensitive to the details of the hadronic interactions along many steps of the cascade, like the multiplicity of the secondaries and the fraction of electromagnetic component with respect to the total signal. On the contrary, the intrinsic muon fluctuations mostly depend on the first interactions. Clear evidence for a deficit of the number of muons predicted by the models was reported by the Auger Collaboration by exploiting different techniques such as the study of inclined showers [48], comparison of the development of the lateral and longitudinal profiles of showers with models [49], the study of the muon production depth [50] and of the time profiles of the signals recorded with SD [40].

More recently and at lower energies, the deficit of muons in the models was also confirmed by directly measuring the muon content in EAS with an array of underground muon detectors (AMIGA project, see Section 4), while comparing with the $X_{\rm max}$ obtained from FD [55]. The resulting predicted muon content is 38% too low when the hadronic interaction model EPOS-LHC is used, the mismatch increasing to 50% - 53% at the two energies in the case of QGSJetII-04.

Shower-to-shower fluctuations of the muonic component could also be measured with hybrid inclined showers [56], at the same time updating the results on the mean muon number. The expectations for the relative fluctuations are compatible with the experimental results, while models and data show a significant discrepancy in the average muon scale. These results thus suggest that models are describing reasonably well the distribution of energy going into the electromagnetic component after the first interaction, while the discrepancy in the overall muon number should be explained by changes in the characteristics of hadronic interactions at all shower stages.

3.5.2. Atmospheric phenomena: ELVES

ELVES is an acronym for "Emissions of Light and Very low frequency perturbations due to Electromagnetic pulse Sources". They are transient luminous events produced at the base of the ionosphere by the intense electromagnetic pulses emitted during lightning discharges. These intense flashes of light appear in the night sky as rapidly expanding quasi-circular fronts; generated at 80–95 km altitudes, they are visible at distances of several hundred kilometers. The original pulse lasts less than 20 μs, but the propagating light front is visible for a few milliseconds.

The first clear observation of ELVES was made using a high-speed photometer from the Space Shuttle. More recently such phenomena were studied using photometers either based at the ground or on satellites.

After the first serendipitous observation of an ELVES event during an FD shift, further studies, done on a sample of data taken in the period 2008–2011, have shown that the FD is ideally suited for detailed studies of ELVES. A new, modified third level trigger algorithm was implemented in March 2013 to increase the detection and recording efficiency of these events. Since then, a large fraction of these events is regularly recorded, and a new dedicated readout scheme has been gradually improved to allow recording of the light emission, from farther and farther distances [51].

Auger has detected thousands of ELVES events with an unprecedented time resolution of 100 ns. These observations facilitate the study of the frequency of such events and of the correlation with other atmospheric phenomena.

3.5.3. Space weather

Every second, the Pierre Auger surface detectors record the rate of low energy particles detected and report this information to the central data acquisition system. This event rate is related to the flux of low energy Galactic cosmic rays reaching the Earth, which is modulated by the solar activity. Therefore, by measuring with great precision the flux variations, and after correction for atmospheric effects, the Pierre Auger Observatory is able to contribute to the Space Weather program, in a way similar to neutron monitors.

A description of the Pierre Auger low energy detection mode can be found in [52]. More information about Space Weather and cosmic rays can be found on the webpage http://www.spaceweather.com/.

4. AugerPrime: The upgrade of the Pierre Auger Observatory

4.1. Science case for the upgrade

So far, the Pierre Auger Observatory has provided important results regarding the upper end of the cosmic ray spectrum, the spectral features at lower energy, the search for anisotropies at different angular scales and the composition of the primaries. However, these findings open up new questions and a full, integrated picture is still missing. Having established the existence of a sharp steepening of the cosmic ray spectrum at the highest energies, it is natural to inquire about the origin of this suppression. It may be due to energy losses during propagation of the cosmic rays from their sources to the Earth, but it could also be an indication of the upper limit of the power of the accelerating sources. Also, the spectral features at lower energy could be an indication of the transition from galactic to extragalactic origin or it may be due to propagation losses. Therefore, for a full understanding of the observations, a combined analysis of the spectrum and the composition is required. Although anisotropies in the arrival directions have been found, the search for the sources is still not concluded. Hints towards a heavier composition at higher energies suggest greater magnetic deflections, which hinders the search for point sources. If, however, even a small fraction of cosmic rays of the highest energies is composed of protons, identifying these protons might lead to a possible indication of the sources. The measurement of the fraction of protons is a decisive ingredient for assessing the prospects for proton astronomy with future ultra-large detectors.

Determining the mass composition of ultra-high energy cosmic rays is closely related to, and crucially depends on understanding extensive air showers and hadronic interactions. When estimating the number of muons in air showers from Auger data, a discrepancy is currently found between the observed and expected muon numbers. The study of extensive air showers and hadronic multiparticle production is a further open field of research, including the exploration of fundamental particle physics at energies well beyond those accessible at terrestrial accelerators as well as the derivation of constraints on new physics phenomena, such as Lorentz invariance violation or extra dimensions.

In 2015, the Pierre Auger Collaboration agreed to design and build an upgrade of the Observatory to address the open science questions described above. The Upgrade is described in [53, 54]. To accomplish its science objectives, it will be of paramount importance to improve the composition sensitivity and to extend it into the energy region of the flux suppression. This will allow us to:

- measure the composition-discriminated flux in the range from about 10^{18} eV up to the highest energies,
- carry out composition-enhanced anisotropy searches based on event-by-event estimates of the primary mass,
- search for GZK secondaries as tracers of proton primaries,
- search for ultra-high energy secondary photons produced in or near cosmic ray sources,
- understand the muon deficit in shower simulations,
- test our understanding of hadronic interactions at c.m.s. energies near and beyond 60 TeV.

Presently, determinations of the cosmic ray mass composition are performed by direct observations of the shower maximum X_{max} with the FD, and indirectly by measuring X_{max} using the surface detectors. Optical observations of X_{max} can currently be performed with a duty cycle of only 13% to 15%. Another good indicator of the primary composition is the number of muons N_μ present in the shower. Therefore, disentangling the muonic and electromagnetic component of the EAS at the ground provides the largest boost in performance towards the aforementioned science goals. This can be achieved either with a muon detector or a detector which has differential sensitivity to both EAS components.

The Pierre Auger Observatory Upgrade, named "AugerPrime", will be based on the following improvements:

- A complementary measurement of the shower particles will be provided by plastic Surface Scintillator Detectors (SSD) placed above the existing 1660 water-Cherenkov Detectors (WCD).
- The surface detector stations will be upgraded with new electronics that will process both WCD and SSD signals. The new electronics will also provide faster sampling of ADC traces, better timing accuracy, increased dynamic range, and enhanced triggers.
- To increase the dynamic range, each WCD will be equipped with an additional "small PMT", i.e., a smaller low gain photomultiplier tube, to register large pulses from very close showers that saturate the signal of the large PMTs.
- An Underground Muon Detector (UMD) will provide important direct measurements of the shower muon content and its time structure, while serving as verification and fine-tuning of the methods used to extract muon information with the SSD and WCD measurements.
- The operation mode of the Fluorescence Detector (FD) will be changed to extend measurements into periods with higher night sky background and twilight. This will allow an increase in the current $\sim$15% duty cycle of the FD to over $\sim$20%.
- Each Surface Detector station will be complemented with an antenna for radio detection of cosmic ray showers.

Both the scintillator planes, the new electronics and the radio antennas can be deployed over the full 3000 km^2 area of the Pierre Auger Surface Detector, with minimal impact on the continuous data taking and maintenance of the existing detectors. Except for the Infill area, the current communication systems for the Surface Detector will remain unchanged. The solar power system will be upgraded with larger, more efficient solar panels. Only minor software changes are required for the central data acquisition system (CDAS) and for the monitoring system.

Prototyping of the Upgrade began in 2015 and its complete installation is planned for 2022. It is expected to operate and provide data for over a decade, nearly doubling the statistics with respect to the presently available one.

4.2. Scintillator Surface Detector (SSD)

The key element of the upgrade is the installation of a new detector consisting of a plastic scintillator plane above each of the existing water-Cherenkov detectors. These scintillation detectors will provide a complementary measurement of the shower particles: as the SSD and the WCD have different responses to muons and electromagnetic particles, this allows for the disentangling of the different shower components. Whereas in a WCD the signal deposited by electromagnetic particles (e^+, e^-, γ) is proportional to their energy and the signal from muons is proportional to their track length, in the SSD each particle contributes essentially one MIP (Minimum Ionizing Particle) to the signal. The SSD array will also map the lateral footprint of EAS at the surface, being more sensitive to the electromagnetic component than to muons.

The design of the surface scintillator detectors is simple and reliable [53]. The SSD unit consists of a box of 3.8 m $\times$ 1.3 m, housing two scintillator panels, each covering an area of 1.9 m^2. Each panel is composed of 24 bars of 10 mm thick, 50 mm wide and 1.6 m long scintillator made of extruded polystyrene. The bars are co-extruded with a TiO2 outer

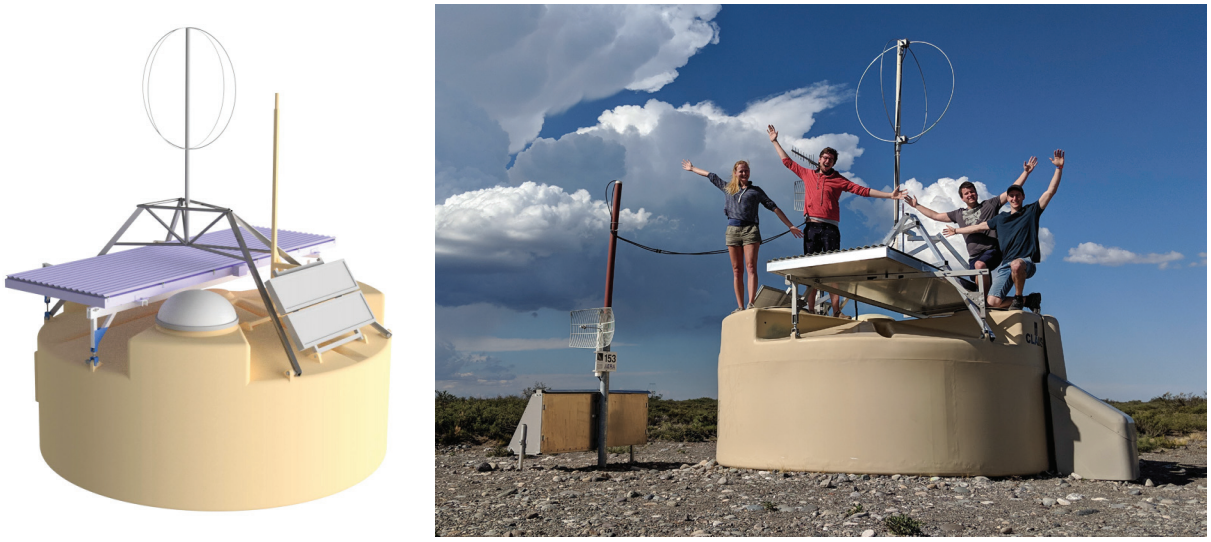

Figure 9. The Pierre Auger Observatory Upgrade: a prototype of an upgraded Auger Surface Detector, including the SSD on top of the tank and the SALLA antenna for the Radio Upgrade. Left: schematics. Right: the detector in the field.

layer for reflectivity and have two holes in which the wavelength-shifting fibres can be inserted. The fibres are 1 mm in diameter and are disposed in a "U" configuration that maximizes light yield and uniformity. The response over the area of the scintillator has been characterised and found to be uniform within 5%. All ends of the fibres are bundled towards one single photomultiplier in the centre of the module. A PMT of 38 mm in diameter, eight stages, fast time response and high linearity was chosen. The triggering of the SSDs is done in slave mode, i.e. the SSD data is read out every time the corresponding WCD reports a trigger.

The SSD modules are easily deployed in the field with a truck and crane. They are fixed to an aluminium frame mounted on top of the WCD tanks of the SD.

Calibration of the SSDs is performed in a similar way as for the WCDs. In a histogram of background signals, a clean peak is observed corresponding to Minimum Ionizing Particle (MIP) signals.

An engineering array of ten detectors was installed at the Auger site in September 2016. First, very encouraging results can be found in [34]. Additional 70 SSDs were installed in the field in 2018 and are collecting data since then. As of August 2020, all of the 1500 SSDs for the Upgrade have already been built at laboratories in Germany, Italy, Poland, Netherlands and France. More than half of them have already been shipped to Malargüe, where they were assembled and installed in the field, awaiting the delivery of the optical modules and electronics. Fig. 9 shows a detector in the field with the SSD installed on top.

4.3. Upgraded electronics

The surface detector stations will be upgraded with new electronics that will process both WCD and SSD signals [53]. It will increase the data quality with faster sampling of ADC traces (120 MHz), giving a better timing accuracy, and increased dynamic range (12 bits). To enhance the local trigger and processing capabilities a more powerful local station processor and FPGA have been implemented. This upgrade also improves calibration and monitoring capabilities of the surface detector stations. The surface detector electronics upgrade (SDEU) can be easily deployed and will have only minimal impact on the continuous data taking of the Surface Detector.

To increase the dynamic range of the WCD, a fourth PMT, 1 inch in diameter, corresponding to 1/9th of the WCD PMTs, will be added in each detector. With this solution, the total dynamic range of the SD will correspond to 22 effective ADC bits, ranging from fractions of 1 VEM (energy from one Vertical Equivalent Muon) to 20,000 VEM. This amplitude in ranges is achieved by splitting and amplifying the anode signal of the three large PMTs of the WCD and by using the single channel of the small additional PMT. This leads to less than 2% saturated events at the highest energies and unambiguous determination of the particle density down to less than 300 m from the shower core.

4.4. AMIGA: Auger muons and infill for the ground array

4.4.1. Underground muon detectors

In addition to the SD array of 1600 WCDs with a 1500 m spacing and the denser array of 61 WCDs with a 750 m spacing (SD-750), more recently the SD energy threshold has been further extended down to $10^{16.5}$ eV thanks to the installation of an even denser 1.9 km^2 array in which detectors are spaced by 433 m (SD-433). To provide a direct measurement of the muon content in air showers, an underground muon detector (UMD) [53] is also being deployed. Both arrays, the "infilled" array of WCDs working jointly with the UMD, form "AMIGA".

The UMD will consist of an array of scintillator detectors co-located at the position of each infill WCD: three 10 m^2 scintillation modules are buried at a distance of at least 7 m from the WCD, at a depth of 2.3 m underground. The separation from the surface detector guarantees that even particles with zenith angles up to 45° hit the underground scintillators without passing through the WCD, while probing the same point in the shower front. The chosen depth, which corresponds to 540 g/cm^2 of overburden as determined by the local soil density, ensures that the electromagnetic component of extensive air showers is largely absorbed while muons with energy greater than 1 GeV can reach the buried detectors. Each underground module is composed of 64 plastic-scintillation strips of 400 cm×1 cm×4 cm, similar to those of the SSD. They carry embedded wavelength-shifting (WLS) optical fibres which are optically coupled to an array of 64 silicon photomultipliers (SiPMs) [57, 58]. The light produced in the plastic scintillation bars is absorbed by the WLS optical fibre. The excited molecules of the fibre decay by emitting photons, some of which are propagated along the fibres towards a single pixel of the array of optical sensors.

Using data of the UMD engineering array that was operative until the end of 2017, it was determined for the first time with direct measurements of the muons, that the muonic densities in data are larger than those expected from simulations of showers between $10^{17.5}$ eV and 10^{18} eV [59], even after the update of the simulations to the latest hadronic interaction models, which include the data from the Large Hadron Collider. After the engineering array phase, modifications in the design were implemented to optimize the detector performance based on the experience gained with the operation of the prototypes. In particular, the optical devices were changed. The formerly used photomultiplier tubes were replaced by silicon photomultipliers to improve the detection efficiency, lower the costs and reduce the power consumption. Additionally, upgraded electronics with a novel acquisition mode to extend the dynamic range were adopted. It was also decided to work with a segmentation per position corresponding to 192 channels total, by splitting the 30 m^2 module into three 10 m^2 units.

A scheme of the layout of an AMIGA station as deployed during the engineering phase is shown in Fig. 10. For the full array, only three buried modules per position will be installed. As of the time of writing this review, the modules at 20 positions were already deployed at the Observatory site, and 15 of them are acquiring data. The completion of the UMD is foreseen for 2022.

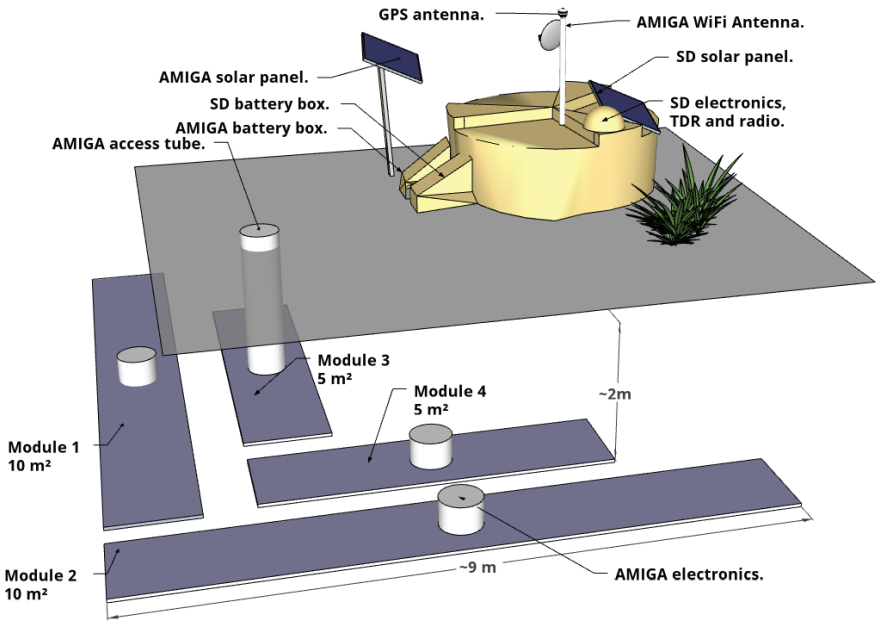

Figure 10. AMIGA station general overview. Both surface and underground detectors are shown in their arrangement during the prototyping phase. For the final design, the 30 m^2 detection area will be reached with three 10 m^2 units with 64 segments each, totalling 192 channels.

4.4.2. Mechanics and electronics of the underground muon detectors

Much effort was invested in developing the buried scintillator detectors that act as muon counters. As can be seen in the left panel of Fig. 11, in each module of the UMD, the scintillator strips are laid in two groups of 32 scintillator bars mounted at opposite sides of a central dome, which houses the optical sensors and the underground electronics. The scintillation light transported by the WLS optical fibre (Saint-Gobain BCF-99-29AMC) is fed to the array of 64 SiPMs, which converts the light pulses into a measurable electrical signal.

Each SiPM of the UMD (Hamamatsu S13361-2050) is composed of 1584 avalanche photodiodes (also referred as *cells*) operated in Geiger mode. The cells are distributed over an area of 2 mm^2 [58]. An electronics board acquires the signals from the photo-sensor and, at the same time, provides control, monitoring and communications to the UMD station.

Figure 11. (Left) A 10 m^2 module being assembled and (Right) its deployment at the Observatory site.

The UMD aims at measuring a broad range of muon densities, from 0.03 m^{-2}, typical for distances far from the shower core, to more than 20 m^{-2} in regions closer to the core where the muon flux is very high. This ample dynamic range is attained by *binary* and *ADC* acquisition modes working simultaneously. The former is optimized to count a small number of particles, the latter is designed to cope with large muon densities.

The binary mode benefits from the detector segmentation: muons can be directly counted as pulses above a certain threshold. This mode is very robust since it neither relies on deconvoluting the total number of particles from a single integrated signal, nor on the precise optical device gain or its fluctuations, and is almost completely independent of the hitting position of the particle on the scintillator strip and the corresponding light attenuation along the fibre. Another advantage is that it does not require a thick scintillator to control Poissonian fluctuations in the number of photons per impinging muon. However, the binary acquisition is limited by the segmentation itself: two muons arriving at the same strip simultaneously will be indistinguishable and, therefore, only counted as one. This undercounting feature is known as *pile-up* effect. As long as the number of strips with coincident signal is less than the segmentation, the pile-up effect can be statistically treated and corrected for, but when the number of particles is similar to the number of channels (64 in this case), the binary mode is saturated and the correction is no longer feasible.

On the other hand, knock-on electrons from the soil or from inclined muons might produce signals in two neighbouring strips resulting in an over-count of particles as well as an increased probability of saturating the detector. Therefore, being limited in the number of muons that can be detected at the same time, the binary mode is limited in the distance to the shower core that can be probed.

To overcome this difficulty, the ADC mode is well-suited to measure a higher number of particles. This mode provides a single, integrated signal from all 64 strips in a module. Contrary to the binary acquisition, in the ADC mode the fluctuations in the signal charge decrease with the number of hitting muons. The disadvantage of the ADC channel, when used to estimate the number of particles, is that it relies on an averaged charge estimation and therefore the signal fluctuations are propagated to uncertainties in the estimation of the muon densities.

In the binary acquisition mode, the 64 SiPM signals are handled independently through a pre-amplifier, a fast shaper, and a discriminator, built within each channel of two 32-channel Application-Specific Integrated Circuits (ASICs). The discriminator signal is sampled at 320 MHz (3.125 ns sample time) with the FPGA into 64 traces of 2048 bits. In each trace, a "1"-bit results if the fast-shaper output is above a fixed discriminator threshold, and a "0"-bit otherwise. The threshold is defined, as last step of the calibration procedure, to significantly reject the noise due to the SiPM dark-counts [58] while keeping a high efficiency.

The data acquisition system of each UMD module is fully synchronized with its associated SD station. Each module works as a slave detector and, therefore, follows the SD trigger chain [27]. The buried scintillators are synchronized at the first-level trigger: when such a condition is met, the WCD sends a signal with a timestamp to all the underground detector modules associated to it. Upon arrival of such signal, the traces of both, binary and ADC modes, as well as the timestamp of the trigger, are stored in an internal memory which can accommodate data up to 2048 triggers. Therefore, the rate of triggers determines that, at each position, the data is retrievable up to $\sim$20 s after its occurrence. Each triggered event in the UMD is composed, in turn, of 2048 samples of 64 single end lines measured at 320 MHz and 1024 samples of two 14-bit ADCs (high and low gain) measured at 160 Msps. The temporal length of each event is 6.4 microseconds and occupies 184 Kbits of memory. When a shower trigger takes place, all first- and second-level triggers from the WCDs, along with the muon detector traces, are sent to the central data acquisition server for higher level physical analysis.

4.5. Radio detection array

Extensive air showers are composed of charged particles undergoing acceleration in the atmosphere and are therefore known to produce radio emission in the frequency range of tens to hundreds of MHz. Radio emission from cosmic rays is due to two effects: the radiation arising from time-varying transverse currents induced by the geomagnetic field and the Askaryan effect related to a time-varying net negative charge. At the Auger Observatory, radio emission was first studied with the Auger Engineering Radio Array (AERA), an array of more than 150 radio detector stations, covering an area of about 17 km^2, co-located with the infill array, see [60, 61] and references therein.

The Auger Upgrade will also include a radio-detector array the size of the SD [62]. Each of the 1660 WCDs will carry a radio antenna on top of it, forming a radio-array covering 3000 km^2 and measuring in coincidence with the SD, the FD (during its uptime fraction of $\sim$15%) and the AMIGA underground muon detectors in the infill area. Fig. 9 shows the layout of the WCD with the SSD and the radio antenna on top of it.

With the combination of water-Cherenkov detector and Surface Scintillator Detector, the electron-to-muon ratio (e/μ) is measured for vertical showers. In a similar way, the combination of WCD and Radio Detector will be used to measure the ratio of the electromagnetic energy content and the number of muons for horizontal air showers. Thus, the Radio Detector will increase the aperture of the Observatory for mass-sensitive investigations, allowing the e/μ separation for showers with a broad zenith angle range, from zenith with the Surface Scintillator Detector to the horizon with the Radio Detector. Horizontal air showers have a large footprint of the radio emission on the ground, covering areas of the order of 100 km^2 for very inclined showers. This has already been confirmed experimentally with AERA. Thus, the radio emission from such showers can be recorded with a sparse antenna array with 1.5 km spacing.

The chosen design proposes the use of a short aperiodic loaded loop antenna (SALLA) to detect the radio emission from air showers in the frequency range 30 to 80 MHz. The SALLA realizes a Beverage antenna as a dipole loop of 1.2 m diameter. The SALLA has been developed to provide a minimal design that fulfills the need for both, ultra-wideband sensitivity, and low costs for production and maintenance of the antenna in a large-scale radio detector. The compact structure of the SALLA makes the antenna robust and easy to manufacture. Beverage antennas include a resistor load within the antenna structure to give a specific shape to the directivity. In the case of the SALLA, a resistance of 500 Ω connects the ends of the dipole arms at the bottom of the antenna. The antenna is read out at the top which is also the position of the Low-Noise Amplifier (LNA). While signals coming from above will induce a current directly at the input of the amplifier, the reception from directions below the antenna is strongly suppressed as the captured power is primarily consumed within the ohmic resistor rather than amplified by the LNA. The resulting strong suppression of sensitivity towards the ground reduces the dependence of the antenna on structures installed below it (like the Surface Scintillator Detector and the water-Cherenkov detector) and on environmental conditions which might vary as a function of time and are thus a source of systematic uncertainty. With the inclusion of an ohmic resistor, the SALLA especially challenges its amplifier as only $\sim$10% of the captured signal intensity is available at the input of the LNA. Proper matching between the antenna structure and the LNA is realized with a 3:1 transmission line transformer. The structure of the SALLA creates a sensitivity which is flat as a function of frequency. The antenna measures along two polarization directions oriented orthogonal to each other. The signals of the two analogue channels will be pre-amplified in a LNA at the antenna. The signals are transmitted through shielded coaxial cables to the filter amplifier on the front-end board. They will be digitized with a sampling frequency of 200 Msps. A FPGA controls the data flow and the communication with the existing electronics of each Surface Detector station.

The water-Cherenkov detector will provide a trigger signal when energy deposition is detected. The data from the radio antenna will be passed to the read-out electronics of the Surface Scintillator Detector/water-Cherenkov detector system (UUB) and will be transmitted together with all data from the station to the central data acquisition of the Auger Observatory.

The expected number of cosmic rays for the envisaged lifetime of the Radio Detector of ten years is of more than 3000 cosmic rays at energies exceeding 10^{19} eV, and approximately of 300 air showers with an energy in excess of $10^{19.5}$ eV. It is to be noticed that an increase of the assumed detection threshold mostly affects detection efficiencies and thus event rates at energies below 10^{19} eV. The Radio Detector will be a powerful tool to study the muon content in inclined air showers. The almost pure separation of the muon content (water-Cherenkov detectors) and electromagnetic energy (radio antennas) of inclined air showers will allow us to determine the energy dependence of the number of muons in inclined air showers, as has previously been done with the combination of water-Cherenkov Detectors and Fluorescence Detectors (FD). The Radio Detector, however, will achieve an order of magnitude higher event statistics: To date, a few hundreds of hybrid FD-SD events above $10^{18.8}$ eV have been collected for this analysis. Over the lifetime of the Radio Detector, roughly 6500 air showers can be collected in that energy range.

Prototypes of all components are installed in the field and evaluation of their performance is ongoing. Mass production of some components has already begun in 2020. The plan foresees to complete the deployment of the almost 1700 units of the 3000 km^2 Radio Detector at the beginning of 2022. The Radio Detector will improve the science capabilities of the Auger Observatory, by providing electron-muon separation for inclined air showers up to the highest energies. This implies also a larger mass-sensitive set of cosmic rays, measured by the Auger Observatory in the overlap region on the sky with the Telescope Array. The Auger Radio Detector is a natural next step towards future cosmic ray experiments,

applying the radio technique on even larger scales, such as GRAND [63] or a next-generation cosmic ray experiment, or applying hybrid detection techniques by combining radio antennas with e.g. segmented water-Cherenkov detectors. The Auger Radio Detector will be the biggest array for the next decade, and it will allow to evaluate the detector technology, establish reconstruction methods, and study the physics performance of such large radio arrays.

Conclusions

The construction of the Pierre Auger Observatory was completed in 2008. It has been running smoothly with nearly full aperture, and has now accumulated more than 12 years of data with the full-size observatory, which allowed to confirm previous results and to provide new insights about the spectrum, arrival directions and mass composition of ultra-high energy cosmic rays. It has also contributed to the understanding of cosmic ray shower physics, high-energy particle interactions, atmospheric phenomena and instrumentation development. The main scientific results have been described in Section 3.

The day-to-day operation of the Observatory demands 34 people on site, mostly highly qualified engineers and technicians. Night shifts for running the Fluorescence Detectors are covered by members of the international collaboration, both on site in Malargüe, as well as in the different control rooms set up at many participating institutions.

A major upgrade of the Auger Observatory is now underway. Presently, more than half of the 1500 SSD have been installed in the field, most of the remaining ones are already in Malargüe awaiting deployment. Their PMTs are being fabricated and tested in Europe and will soon be shipped to the site for installation. Small PMTs for increased dynamic range of the WCDs are ready to be deployed together with the new electronics. An engineering array of more than 70 SSD is running for more than a year in the field, using the original electronics kits. Their performance indicates that they respond according to design. The first batch of the preproduction series of upgraded electronics is being tested and will be installed at the site in the coming months. The upgrade of the Pierre Auger Observatory is expected to be completed in 2022.

AugerPrime, the Upgrade of the Pierre Auger Observatory, will provide a multi-hybrid cosmic ray detector, that will allow simultaneous measurement of a shower with water-Cherenkov detectors, surface scintillator detectors, radio detectors, muon counters and fluorescence detectors. As an illustration of the potentiality of this approach, in Fig. 12 a real event with the measured signals of all the surface techniques is shown. Operation of the upgraded Observatory is expected for at least 10 years.

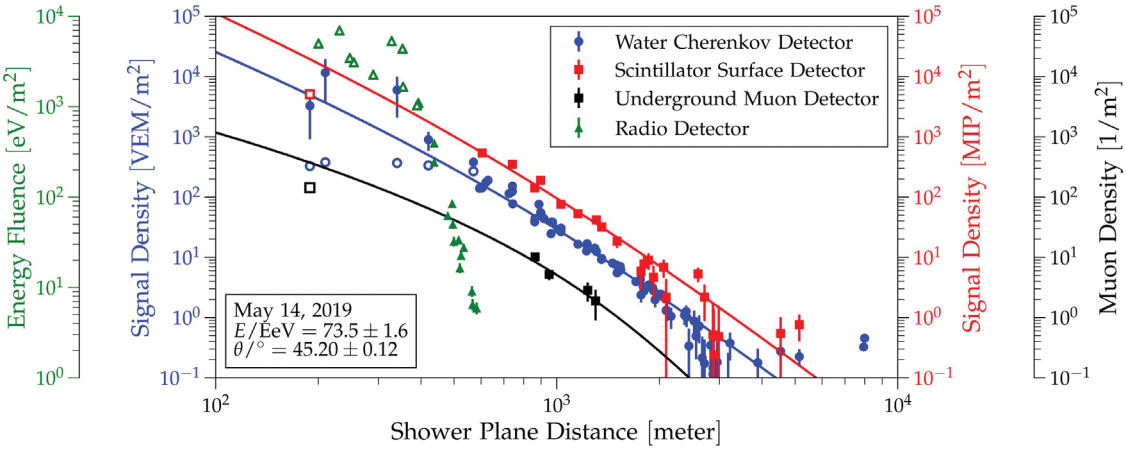

Figure 12. Lateral distribution of signals from SD, SSD, UMD and RD of a real event, as a function of the distance to the reconstructed shower core, including a fit (solid red, blue and black lines) to the measured data.

Outreach to the local community is important for the Auger Collaboration. The Visitor Centre in the town of Malargüe has already received more than 120,000 visitors, including many schoolchildren from the town of Malargüe and the Province of Mendoza. A webpage www.auger.org is maintained to provide updated news and information on the Observatory. Public data for outreach and educational purposes is also provided through that page.

Acknowledgments

The successful installation, commissioning, and operation of the Pierre Auger Observatory would not have been possible without the strong commitment and effort from the technical and administrative staff in Malargüe. We are very grateful to the following agencies and organizations for financial support:

Argentina – Comisión Nacional de Energía Atómica; Agencia Nacional de Promoción Científica y Tecnológica (ANPCyT); Consejo Nacional de Investigaciones Científicas y Técnicas (CONICET); Gobierno de la Provincia de Mendoza;

Municipalidad de Malargüe; NDM Holdings and Valle Las Leñas; in gratitude for their continuing cooperation over land access; Australia – the Australian Research Council; Brazil – Conselho Nacional de Desenvolvimento Científico e Tecnológico (CNPq); Financiadora de Estudos e Projetos (FINEP); Fundação de Amparo à Pesquisa do Estado de Rio de Janeiro (FAPERJ); São Paulo Research Foundation (FAPESP) Grants No. 2019/10151-2, No. 2010/07359-6 and No. 1999/05404-3; Ministério da Ciência, Tecnologia, Inovações e Comunicações (MCTIC); Czech Republic – Grant No. MSMT CR LTT18004, LM2015038, LM2018102, CZ.02.1.01/0.0/0.0/16_013/0001402, CZ.02.1.01/0.0/0.0/18_046/0016010 and CZ.02.1.01/0.0/0.0/17_049/0008422; France – Centre de Calcul IN2P3/CNRS; Centre National de la Recherche Scientifique (CNRS); Conseil Régional Ile-de-France; Département Physique Nucléaire et Corpusculaire (PNC-IN2P3/CNRS); Département Sciences de l'Univers (SDU-INSU/CNRS); Institut Lagrange de Paris (ILP) Grant No. LABEX ANR-10-LABX-63 within the Investissements d'Avenir Programme Grant No. ANR-11-IDEX-0004-02; Germany – Bundesministerium für Bildung und Forschung (BMBF); Deutsche Forschungsgemeinschaft (DFG); Finanzministerium Baden-Württemberg; Helmholtz Alliance for Astroparticle Physics (HAP); Helmholtz-Gemeinschaft Deutscher Forschungszentren (HGF); Ministerium für Innovation, Wissenschaft und Forschung des Landes Nordrhein-Westfalen; Ministerium für Wissenschaft, Forschung und Kunst des Landes Baden-Württemberg; Italy – Istituto Nazionale di Fisica Nucleare (INFN); Istituto Nazionale di Astrofisica (INAF); Ministero dell'Istruzione, dell'Universitá e della Ricerca (MIUR); CETEMPS Center of Excellence; Ministero degli Affari Esteri (MAE); México – Consejo Nacional de Ciencia y Tecnología (CONACYT) No. 167733; Universidad Nacional Autónoma de México (UNAM); PAPIIT DGAPA-UNAM; The Netherlands – Ministry of Education, Culture and Science; Netherlands Organisation for Scientific Research (NWO); Dutch national e-infrastructure with the support of SURF Cooperative; Poland -Ministry of Science and Higher Education, grant No. DIR/WK/2018/11; National Science Centre, Grants No. 2013/08/M/ST9/00322, No. 2016/23/B/ST9/01635 and No. HARMONIA 5–2013/10/M/ST9/00062, UMO-2016/22/M/ST9/00198; Portugal – Portuguese national funds and FEDER funds within Programa Operacional Factores de Competitividade through Fundação para a Ciência e a Tecnologia (COMPETE); Romania – Romanian Ministry of Education and Research, the Program Nucleu within MCI (PN19150201/16N/2019 and PN19060102) and project PN-III-P1-1.2-PCCDI-2017-0839/19PCCDI/2018 within PNCDI III; Slovenia – Slovenian Research Agency, grants P1-0031, P1-0385, I0-0033, N1-0111; Spain – Ministerio de Economía, Industria y Competitividad (FPA2017-85114-P and FPA2017-85197-P), Xunta de Galicia (ED431C 2017/07), Junta de Andalucía (SOMM17/6104/UGR), Feder Funds, RENATA Red Nacional Temática de Astropartículas (FPA2015-68783-REDT) and María de Maeztu Unit of Excellence (MDM-2016-0692); USA – Department of Energy, Contracts No. DE-AC02-07CH11359, No. DE-FR02-04ER41300, No. DE-FG02-99ER41107 and No. DE-SC0011689; National Science Foundation, Grant No. 0450696; The Grainger Foundation; Marie Curie-IRSES/EPLANET; European Particle Physics Latin American Network; and UNESCO.

References

[1] K.-H. Kampert and A. Watson, "Extensive Air Showers and Ultra High-Energy Cosmic Rays: A Historical Review", EPJ-H 37 (2012) 359

[2] G. W. Clark et al, Phys. Rev. 122 (1961) 637

[3] J. Linsley, L. Scarsi and B. Rossi, Phys. Rev. Lett. 6 (1961) 485

[4] J. Linsley, Phys. Rev. Lett. 10 (1963) 146

[5] A. A. Penzias and R. W. Wilson, "A Measurement of Excess Antenna Temperature at 4080 Mc/s", Astrophysical Journal, 142 (1965) 419

[6] K. Greisen, "End to the Cosmic-Ray Spectrum?", Physical Review Letters 16 (1966) 748

[7] G. T. Zatsepin and V. A. Kuz'min,"Upper Limit of the Spectrum of Cosmic Rays", Journal of Experimental and Theoretical Physics Letters 4 (1966) 78

[8] F. W. Stecker and M. H. Salamon, "Photodisintegration of Ultra–High-Energy Cosmic Rays: A New Determination", The Astroph. Journal 512 (1999) 521

[9] L. N. Epele and E. Roulet, "Comment on "On the Origin of the Highest Energy Cosmic Rays"" Phys. Rev. Lett. 81 (1998) 3295

[10] See, for example, http://www.astro.ucla.edu/ rene/talks/Cronin-Fest-Ong-Writeup.pdf

[11] M.M. Winn et al., J.Phys.G: Nucl.Phys., 12 (1986) 653

[12] R. M. Tennent, "The Haverah Park extensive air shower array", Proceedings of the Physical Society 92(2002) 622

[13] A. A. Ivanov et al., New Journal of Physics 11 (2009) 065008

[14] The KASCADE-Grande Collaboration, Nuclear Instruments and Methods in Physics Research A 620 (2010) 202

[15] N. Hayashida et al., Astropart. Phys. 10 (1999) 303

[16] R. M. Baltrusaitis et al., "The Utah Fly's Eye detector", Nuclear Instruments and Methods in Physics Research A 240 (1985) 410

[17] T. Abu-Zayyad et al., Proc. 26th ICRC, 4 (1999) 349

[18] J. H. Boyer et al., Nucl. Inst. Meth. A 482 (2002) 457

[19] D. J. Bird et al., "Detection of a cosmic ray with measured energy well beyond the expected spectral cutoff due to cosmic microwave radiation", The Astrophysical Journal 441 (1995) 144

[20] M. Takeda et al., Astropart. Phys. 19 (2003) 447

[21] R. U. Abbasi et al., Physical Review Letters 100 (2008) 101101; R. U. Abbasi et al., Astroparticle Physics 32 (2009) 53

[22] I. Allekotte et al. [The Pierre Auger Collaboration], "Site survey for the Pierre Auger observatory", J. Phys. G: Nucl. Part. Phys. 28 (2002) 1499

[23] H. Kawai et al., "Telescope Array Experiment", Nuclear Physics B Proceedings Supplements 175–176 (2008) 221

[24] The Pierre Auger Collaboration, "The Pierre Auger Cosmic Ray Observatory", Nuclear Instruments and Methods in Physics Research A 798 (2015) 172

[25] The Pierre Auger Collaboration, "Properties and performance of the prototype instrument for the Pierre Auger Observatory", Nuclear Instruments and Methods in Physics Research A: 523 (2004) 50

[26] I. Allekotte et al. [The Pierre Auger Collaboration], "The surface detector system of the Pierre Auger Observatory", Nuclear Instruments and Methods in Physics Research A 586 (2008) 409

[27] The Pierre Auger Collaboration, "Trigger and aperture of the surface detector array of the Pierre Auger Observatory", Nuclear Instruments and Methods in Physics Research A 613 (2010) 29

[28] X. Bertou et al., Nuclear Instruments and Methods in Physics Research A 568 (2006) 839

[29] The Pierre Auger Collaboration, "Reconstruction of Events Recorded by the Surface Detector of the Pierre Auger Observatory", accepted by JINST (2020)

[30] J. Abraham et al. [The Pierre Auger Collaboration], "The fluorescence detector of the Pierre Auger Observatory", Nuclear Instruments and Methods in Physics Research A 620 (2010) 227

[31] V.Verzi [Pierre Auger Collaboration], "Measurement of the energy spectrum of ultra-high energy cosmic rays using the Pierre Auger Observatory", PoS(ICRC2019) (2019) 450

[32] The Pierre Auger Collaboration, "Features of the energy spectrum of cosmic rays above 2.5×10^{18} eV using the Pierre Auger Observatory", to be published in Phys. Rev. Letters (2020) ; "A measurement of the cosmic ray energy spectrum above 2.5×10^{18} eV using the Pierre Auger Observatory", to be published in Phys. Rev. D (2020).

[33] A. Castellina [Pierre Auger Collaboration], "Highlights from the Pierre Auger Observatory", PoS(ICRC2019) (2019)

[34] The Pierre Auger Collaboration, "Contributions to the 36th International Cosmic Ray Conference (ICRC 2019)", arXiv:1909.09073 (2019)

[35] Telescope Array Collaboration, Astrophys. J. 768 (2013) L1

[36] The Pierre Auger Collaboration, Phys. Rev. Lett. 101 (2008) 061101

[37] D. J. Bird et al. [HiRes Collaboration], Phys. Rev. Lett. 71, 3401 (1993)

[38] The Pierre Auger Collaboration, Phys. Lett. B685 (2010) 239, arXiv:1002.1975 [astro-ph.HE]

[39] T. K. Gaisser, "Cosmic Rays and Particle Physics", Cambridge University Press, Cambridge, 1990

[40] The Pierre Auger Collaboration, "Inferences on mass composition and tests of hadronic interactions from 0.3 to 100 EeV using the water-Cherenkov detectors of the Pierre Auger Observatory", Phys. Rev. D 96 (2017) 122003

[41] The Pierre Auger Collaboration, "Combined fit of spectrum and composition data as measured by the Pierre Auger Observatory", JCAP04 (2017) 038

[42] The Pierre Auger Collaboration, Astrop. J. Lett. 853 (2018) L29

[43] The Pierre Auger Collaboration, Science 357 (2017) 1266

[44] E. Roulet [The Pierre Auger Collaboration], "Large-scale anisotropies above 0.03 EeV measured by the Pierre Auger Observatory", PoS(ICRC2019) (2019) 408

[45] R. Engel, D. Seckel and T. Stanev, "Neutrinos from propagation of ultrahigh energy protons", Phys. Rev. D 64 (2001) 093010

[46] The Pierre Auger Collaboration, "Limits on point-like sources of ultra-high-energy neutrinos with the Pierre Auger Observatory", JCAP 11 (2019) 004; F. Pedreira [The Pierre Auger Collaboration], "Bounds on diffuse and point source fluxes of ultra-high energy neutrinos with the Pierre Auger Observatory" PoS (ICRC2019) (2019) 979

[47] J. Rautenberg [The Pierre Auger Collaboration], "Limits on ultra-high energy photons with the Pierre Auger Observatory", PoS(ICRC2019) (2019) 398

[48] The Pierre Auger Collaboration, Phys. Rev. D91 (2015) 032003

[49] The Pierre Auger Collaboration, Phys. Rev. Lett. 117 (2016) 192001

[50] The Pierre Auger Collaboration, Phys. Rev. D 90 (2014) 012012; D90 (2014) 039904(A); D92 (2015) 019903(E)

[51] The Pierre Auger Collaboration, "A Three Year Sample of Almost 1600 Elves Recorded Above South America by the Pierre Auger Cosmic Ray Observatory", Earth Space Sci. 7 (2020) e2019EA000582

[52] The Pierre Auger Collaboration, "The Pierre Auger Observatory scaler mode for the study of solar activity modulation of galactic cosmic rays", Journal of Instrumentation, 6 (2011) P01003 (open access)

[53] The Pierre Auger Collaboration, "The Pierre Auger Observatory Upgrade - Preliminary Design Report", arXiv:1604.03637 (2016)

[54] A.Castellina [The Pierre Auger Collaboration], "AugerPrime: the Pierre Auger Observatory Upgrade", EPJ Web Conf. 210 (2019) 06002

[55] F.Sanchez [The Pierre Auger Collaboration], "The muon component of extensive air showers above $10^{17.5}$ eV measured with the Pierre Auger Observatory", PoS (ICRC2019) (2019) 411; Pierre Auger Collaboration, "Direct measurement of the muonic content of extensive air showers between 2×10^{17} and 2×10^{18} eV at the Pierre Auger Observatory", Eur. Phys. J. C (2020) .

[56] F. Riehn [The Pierre Auger Collaboration], "Measurement of the fluctuations in the number of muons in inclined air showers with the Pierre Auger Observatory", PoS(ICRC2019) 404

[57] The Pierre Auger Collaboration, JINST 11 (2016) P02012

[58] The Pierre Auger Collaboration, JINST 12 (2017) P03002

[59] The Pierre Auger Collaboration, "Direct measurement of the muonic content of extensive air showers between 2×10^{17} and 2×10^{18} eV at the Pierre Auger Observatory", Eur. Phys. J. C (2020) to be published

[60] The Pierre Auger Collaboration, "Observation of inclined EeV air showers with the radio detector of the Pierre Auger Observatory " JCAP 10 (2018) 026

[61] T. Huege [The Pierre Auger Collaboration], "Radio detection of cosmic rays with the Auger Engineering Radio Array", EPJ Web Conf. 210 (2019) 05011

[62] B. Pont [The Pierre Auger Collaboration], "A large radio detector at the Pierre Auger Observatory - measuring the properties of cosmic rays up to the highest energies", POS(ICRC2019) (2019) 434

[63] J. Alvarez-Muñiz, et al., Science China: Phys., Mech. & Astron., 63 (2020) 219501; http://arxiv.org/abs/1810.09994